

Chapter - III

Effect of swift heavy ions on physical properties of PMMA/Ag and PS/Ag nanocomposites

Abstract

In this chapter swift heavy ions (120 MeV Si ions, 85 MeV C ions) induced modifications of Silver nanoparticles dispersed PMMA and PS nanocomposites films at the fluences of 1×10^{11} , 1×10^{12} ions/cm² were studied. 120 MeV Si swift heavy ions induced more prominent effects on the physico-chemical properties of polymer nanocomposites compared to those of C-ions. An XRD analysis reveals that the crystallite size of the composites decreased after ion beam irradiation which is also corroborated by the DSC analysis due to the chain scissioning upon irradiation in PMMA nanocomposites. In PS nanocomposites, we observed cross linking upon irradiation. It was observed from the UV- visible spectroscopy analysis that the band gap value moved to the lower energy on doping with metal nanoparticles, as well as upon irradiation. SEM images showed damages upon ion beam irradiation. The dielectric constant of the composites increased with the increase of metal content and also upon ion beam irradiation. These phenomena could be interpreted from interfacial polarization of heterogeneous systems.

3.0 Introduction:

Polymer reinforced with fillers is a common way to achieve improved properties in the fabrication of modern plastics due to their synergistic and hybrid properties derived from several components. Polymer nanocomposites have recently received significant attention because of the new and superior properties (e.g., electrical, thermal, and mechanical) to conventional composites of these materials and may be synthesized using surprisingly simple and inexpensive techniques [1, 2].

Swift heavy ion (SHI) irradiation is a unique post-deposition treatment in view of its ability to modify the polymers properties which are associated with the collisions of penetrating high energy ions with the target atoms and the formation of defects [3]. The defects lead to the change in the structural, optical and electrical transport properties of the materials. These changes are strongly dependent on mass of the incident ions, irradiation energy and fluences. The irradiation may cause ionization or excitation, and possibly displacement of atoms from their sites in the lattice of the materials. Different studies of effect of ion beam irradiation on polymers/polymer composites expose a variety of changes in structural and chemical composition, main-chain scissioning, intermolecular cross-linking, creation of unsaturated bonds, formation of volatile fragments and creation of carbonaceous clusters etc. [4, 5, 6]

So far not much work have been reported which deals with the SHI effect on the nanocomposites. The aim for this work is to produce composites with high dielectric constant and low dielectric loss which is required for telecommunications, microelectronic devices, EMI shielding etc. For that purpose, we have synthesized following polymer nanocomposites and studied the effect of 120 MeV Si ions and 85 MeV C ions on these composites.

- (i) PMMA + Ag [7]

(ii) PS + Ag [8]

Properties and preparation methods of composites have been discussed in chapter 2. All the films were irradiated with 120 MeV Si- ions and 85 MeV C- ions at the fluences of 1×10^{11} , 1×10^{12} ions/cm² at Inter University Accelerator Centre (IUAC), New Delhi, India. We have studied changes in the structural, thermal, optical and dielectric properties of composites due to swift heavy ions irradiation by means of X-ray diffraction, differential scanning calorimetry, UV-visible spectroscopy and impedance gain phase analyzer.

3.1 Effect of swift heavy ions irradiation on PMMA + Ag nanocomposites:

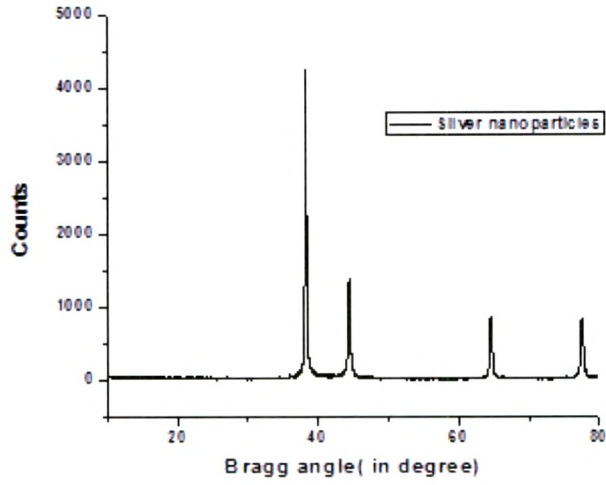
3.1.1 X-ray diffraction analysis:

The diffraction patterns of the pristine and irradiated polymer composites films are shown in Fig. 3.1(a-f). The diffraction peaks of Ag/PMMA composites showed four well defined crystalline peaks at $2\theta = 38.4, 44.3, 64.7$ and 77.6° , corresponding to the (111), (200), (220) and (311) planes of the face-centered cubic (fcc) Ag phase compared with the standard powder diffraction card of Joint Committee on Powder Diffraction Standards (JCPDS), and silver file No. is 04-0783. The broad peak at $2\theta = 14.79$ in the diffraction pattern of the pristine film indicates that the polymer is amorphous in nature. Because of influence of silver nanoparticles in PMMA matrix, it shows semi-crystalline diffraction pattern. It is observed from figure that intensity of diffraction peak varies after both irradiation. The crystallite size has been calculated before and after irradiation using Scherrer's formula (2.2.3) [9] as discussed in chapter 2 in section 2.3.1.

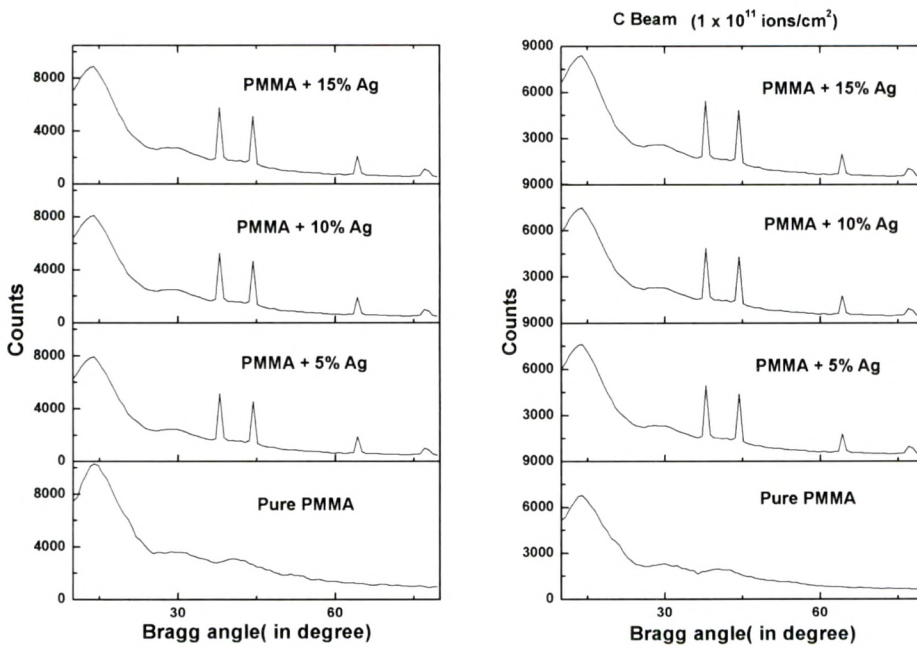
$$b = K\lambda / L \cos\theta$$

where b is FWHM in radians, λ is the wavelength of X-ray beam (1.5418 \AA), L is the

crystallite size in Å, K is a constant which varies from 0.89 to 1.39, but for most of the cases it is close to 1.

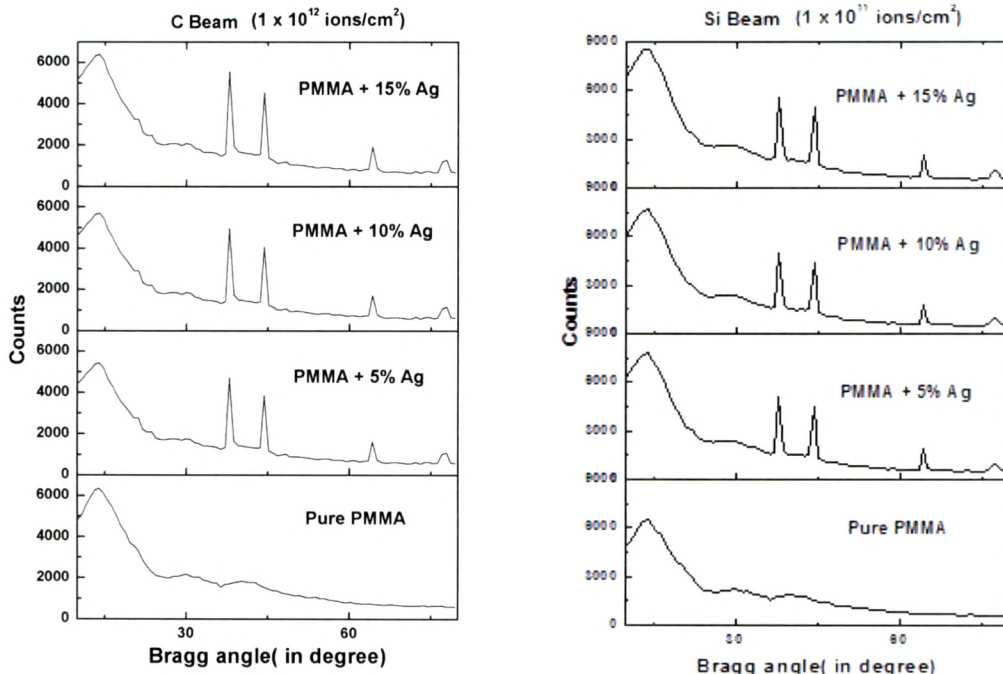


(a)



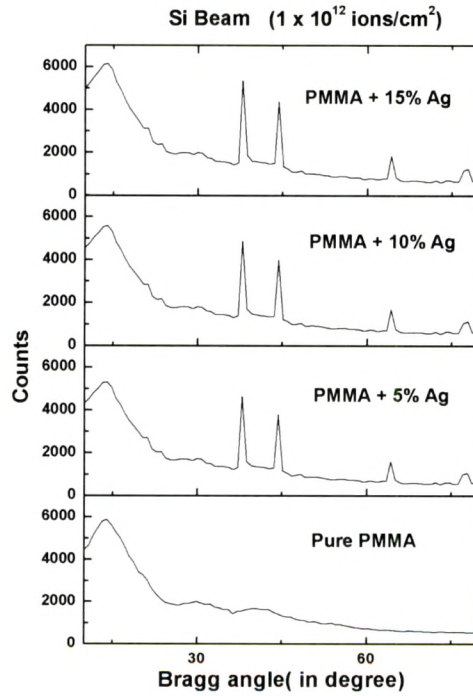
(b)

(c)



(d)

(e)



(f)

Fig. 3.1 X-ray diffraction patterns of (a) silver nanoparticles, (b) PMMA+ Ag (pristine) (C) C beam (1×10^{11} ions/cm²) (d) C beam (1×10^{12} ions/cm²) (e) Si beam (1×10^{11} ions/cm²) (f) Si beam (1×10^{12} ions/cm²)

The appearance of sharp peak in composite indicates some degree of crystallinity. Results show that crystallite size of fillers decreases slightly upon both ion beams irradiations. It is also observed that the intensity of the peak decreases and to some extent broadening of the peak after irradiation offers confirmation of decrease in crystallinity. Since no significant change in the peak position is observed, this reveals that lattice parameters do not change significantly in both irradiations. The broadening of peak suggests an evolution of the polymer towards a more disordered state [10]. The crystallite size was calculated from the relation 2.2.3 as discussed in chapter 2 corresponding to the peak of the pristine and irradiated samples and the results are listed in Table 3.1

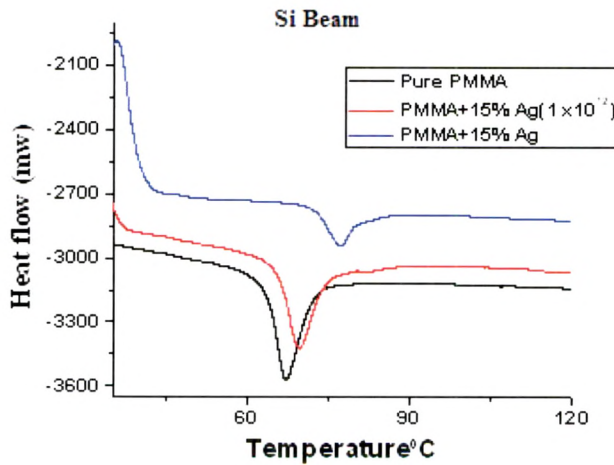
Table 3.1 Crystallite size of pristine and irradiated samples

Sample	Pristine		C Beam		Si Beam	
	2 θ	Crystallite size (nm)	Crystallite size (nm) (1×10^{11}) ions/cm ²	Crystallite size (nm) (1×10^{12}) ions/cm ²	Crystallite size (nm) (1×10^{11}) ions/cm ²	Crystallite size (nm) (1×10^{12}) ions/cm ²
PMMA+ 5%Ag	38.07	32.64	31.61	30.14	31.20	29.98
	44.24	33.17	32.18	30.67	30.34	29.34
	64.23	32.44	30.11	29.10	29.23	28.54
	Average	32.75	31.30	29.97	30.26	29.28
PMMA + 10%Ag	38.05	32.89	31.11	30.34	31.56	29.88
	44.21	33.98	30.21	29.11	29.56	29.34
	64.19	34.23	32.67	31.33	29.33	29.58
	Average	33.70	31.33	30.26	30.15	29.60
PMMA + 15%Ag	38.01	34.24	33.25	31.22	32.89	30.69
	44.18	36.12	34.12	32.78	31.78	30.31
	64.15	38.45	36.78	33.67	30.14	29.45
	Average	36.27	34.72	32.56	31.60	30.15

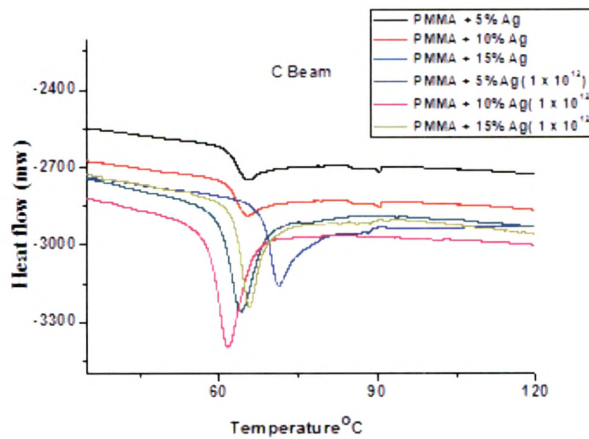
Results show that the ion beam irradiation causes large amount of energy deposition in the material which leads to decrease in crystallite size. It may be attributed to splitting of crystalline grains due to absorption of large amount of energy and it also reflects the formation of disorder system. The irradiation may induce chain scissioning, which is also corroborated by DSC analysis, assumed to be responsible for the reduction in crystallinity of the composite [10].

3.1.2 Thermal response (Differential scanning calorimetry (DSC)):

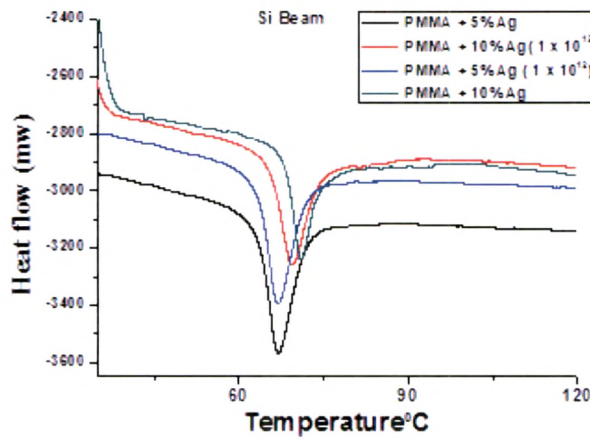
The important property of the polymer is the glass transition temperature (T_g), which is defined as the temperature at which the plastic becomes hard and brittle when cooled rapidly after heating. At the glass transition temperature, the weak secondary bonds that stick the polymer chains together are broken, and the macromolecule starts to move. The influence of silver nanoparticles and irradiation on the glass transition behavior of polymer matrix (PMMA) was investigated with dynamic DSC technique. The values of T_g were taken as the midpoint of the glass transition event and



(a)



(b)



(c)

Fig. 3.2 DSC thermo grams for (a) Pure and composites, (b) Composites for C beam, (c) Composites for Si beam

collected as shown in Fig. 3.2(a, b, c). The pure PMMA has a T_g value of 64.60°C, while tendency of increase of T_g value after inclusion of silver nanoparticles was observed for Ag/PMMA nanocomposites. The interaction of polymer chains and nanoparticles surface can alter the chain kinetics by decreasing or increasing glass transition temperature of the polymer [11]. We found the value of T_g, for pristine and irradiated samples is listed in Table 3.2 for highest fluence of C beam and Si beam.

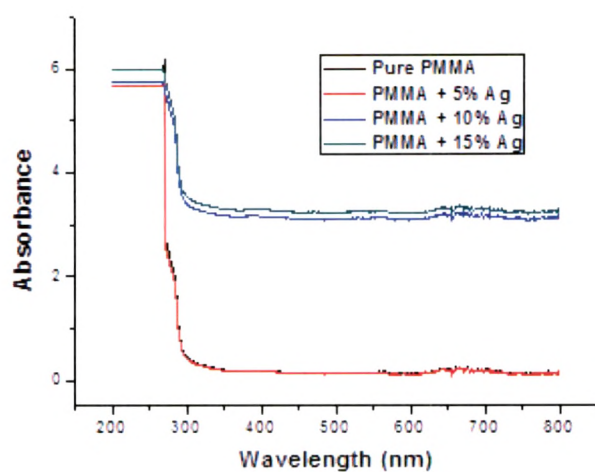
Table 3.2 Values of glass transition for pristine and irradiated composites

Sample name	Tg (Pristine)	Tg (C beam)	Tg (Si beam)
PMMA + 5 %Ag	65.8	64.1	63.1
PMMA + 10 %Ag	66.1	64.8	63.2
PMMA + 15 %Ag	71.4	65.8	64.2

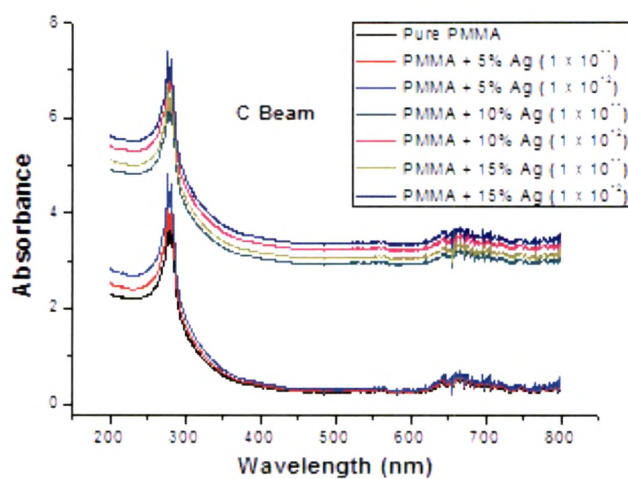
Ash et al [12] explained the decrease of Tg values in terms of thin film model. When the inter-particles distance is small enough, then the polymer between two particles can be considered as a thin film. Assuming that there is small or no interfacial interaction between the filler and matrix exists and then Tg decreases.

3.1.3 Optical response:

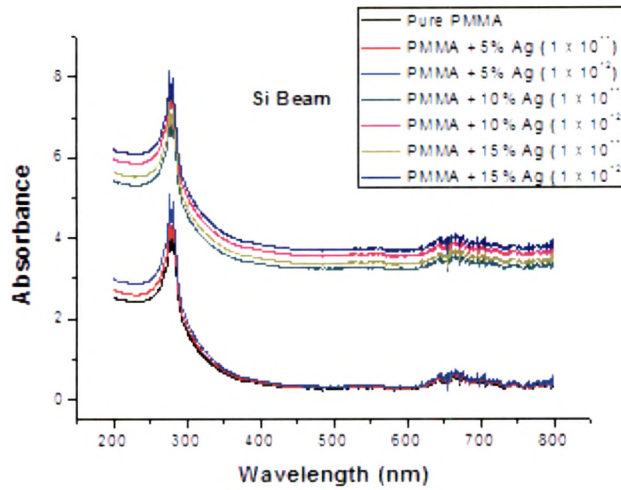
Ultraviolet-visible spectroscopy provides an idea about the optical band-gap energy (E_g), and thus a significant tool for investigation. The absorption of light energy by polymeric materials in the ultraviolet and visible regions involves promotion of electrons in σ , π and n orbitals from the ground state to higher energy states which are explained by molecular orbitals [13]. The following types of electronic transitions $\sigma \rightarrow \sigma^*$, $n \rightarrow \sigma^*$, $n \rightarrow \pi^*$, and $\pi \rightarrow \pi^*$ are involved in the ultraviolet and visible regions. Many of the optical transitions which resulted due to the presence of impurities have energies in the visible part of the spectrum; consequently the defects are referred to as colour centres [14]. The decrease in energy band gap of the composites upon irradiation which leads to the formation of new defects and new charge states, due to breakage of bonds and formation of free radicals, unsaturation etc [15].



(a)



(b)



(c)

Fig. 3.3 Absorbance spectra for (a) pristine (b) irradiated by C-beam (c) irradiated by Si- beam

Determinations of band gap

Optical feature of the pristine and irradiated samples have been studied by Perkin-Elmer 25 Lambda UV-Visible spectroscope in the frequency range 200-800 cm^{-1} as illustrated in Fig.3.3 (a, b, c). The optical band gap E_g is obtained by tauc's equation [16] as discussed in chapter 2 in the section 2.3.3 by the relation 2.2.4.

i. e.
$$\omega\varepsilon(\lambda) = (\hbar\omega - E_g)^2$$

Where $\varepsilon(\lambda)$ is the optical absorbance and λ is the wavelength. The intersection of the extrapolated spectrum with the abscissa of the plot $\varepsilon^{1/2}/\lambda$ versus $1/\lambda$ yields the gap wavelength λ_g from which the energy gap is derived as $E_g = hc/\lambda_g$. It is noticed that the band gap (energy gap) value shifted to lower energy from 4.58 eV upto 3.21 eV due to doping of silver nanoparticles and also upon irradiation. This is because of the scissioning of polymer chain and as a result, creation of free radicals, unsaturation etc. and thus a capability of increasing the conductivity of the composites [17].

The number of carbon atoms per cluster can be calculated by and shown in Table 3.3[14] from the relation 2.2.5 as explained in chapter 2.

$$E_g = 34.3/\sqrt{N} \text{ eV}$$

Where, N is the number of carbon atoms per cluster and E_g is the energy band gap.

Table 3.3 Band gap (B.G) and no. of carbon atoms (N) of pristine and irradiated samples

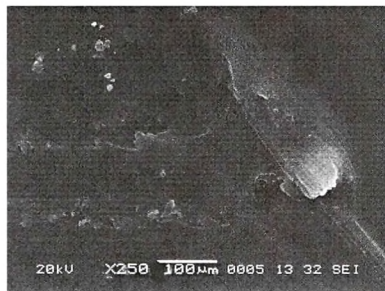
Sample	Pristine	C Beam		Si Beam	
	B.G eV	B.G eV 1×10^{11} ions/cm ²	B.G eV 1×10^{12} ions/cm ²	B.G eV 1×10^{11} ions/cm ²	B.G eV 1×10^{12} ions/cm ²
Pure PMMA	4.58	4.50	4.38	4.36	4.26
PMMA + 5%Ag	4.28	4.21	4.10	4.05	3.87
PMMA + 10%Ag	4.10	4.01	3.89	3.80	3.52
PMMA + 15%Ag	3.82	3.75	3.65	3.61	3.21

Sample	Pristine	C Beam		Si Beam	
	No. of carbon atoms(N)	No. of carbon atoms(N) 1×10^{11} ions/cm ²	No. Of carbon atoms(N) 1×10^{12} ions/cm ²	No. of carbon atoms(N) 1×10^{11} ions/cm ²	No. Of carbon atoms(N) 1×10^{12} ions/cm ²
Pure PMMA	56	58	61	62	65
PMMA + 5%Ag	64	66	70	72	78
PMMA + 10%Ag	70	73	77	81	95
PMMA + 15%Ag	80	84	88	90	114

3.1.4 Surface morphology:

Fig. 3.4(a-f) shows the SEM images of pristine, composites and irradiated (1×10^{12} ions/cm²) composite films with magnification of X250. The analysis shows that the

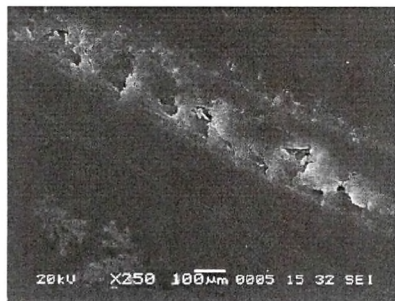
filled particles are distributed randomly in the matrix which display continuous contact between themselves and formed conducting paths. The surface roughness is observed to increase upon irradiation. The increase in roughness with Ag-nanoparticles may be attributed to the increase in density and size of metal particles on the surfaces of the films, which is also responsible for decrease in crystallinity of the material as indicated by XRD analysis [18].



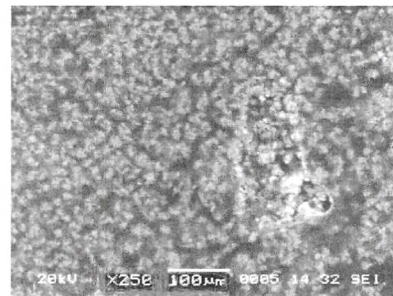
(a)



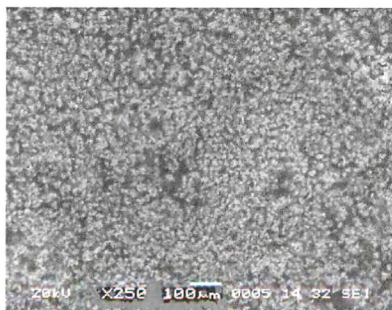
(b)



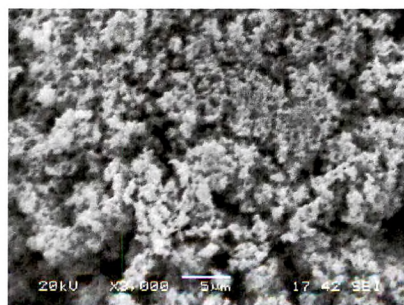
(c)



(d)



(e)



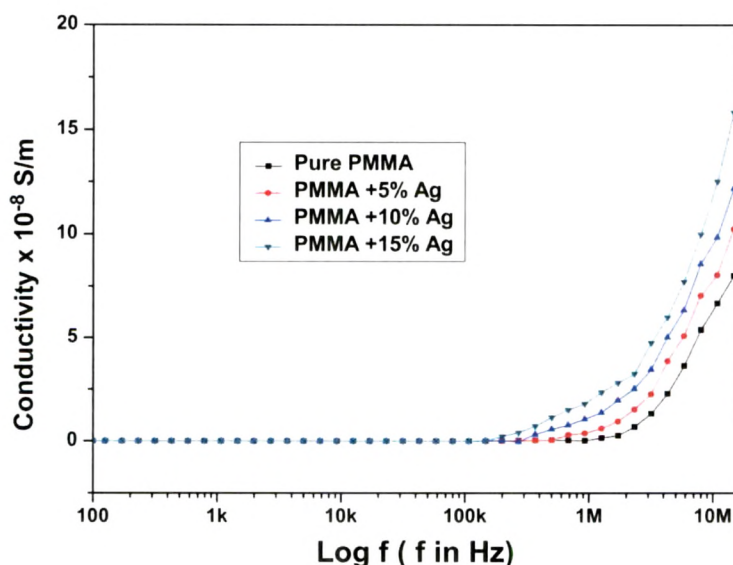
(f)

Fig. 3.4 SEM Images for (a) Pure PMMA (b) PMMA irradiated (C beam) (c) PMMA+15% Ag (d) PMMA+15% Ag (C Beam) (e) PMMA+15% Ag (Si beam) (f) Ag nanoparticles

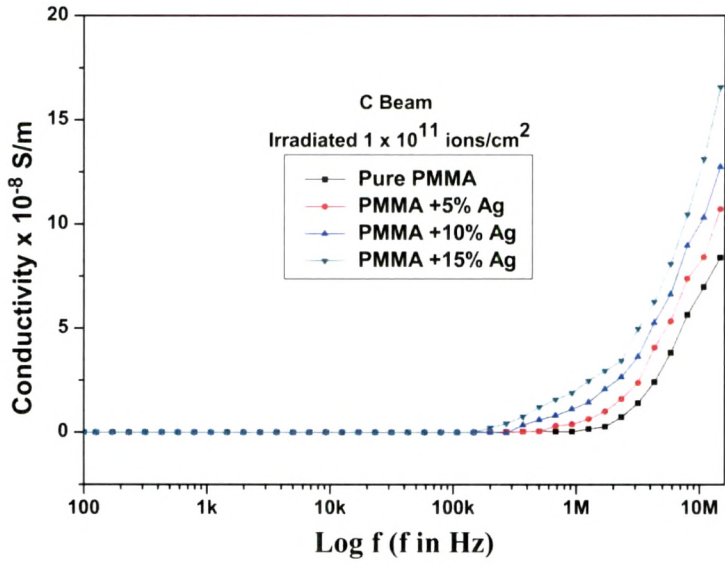
3.1.5 AC Electrical Frequency Response:

Conductivity: AC electrical measurement was carried out for pristine and irradiated samples. The conductivity was calculated by relation (2.2.20) as discussed in chapter 2 in section (2.3.6(a)). Fig. 3.5 (a-e) shows the variation of conductivity with log of frequency for the pristine and irradiated samples at different silver nanoparticles concentrations.

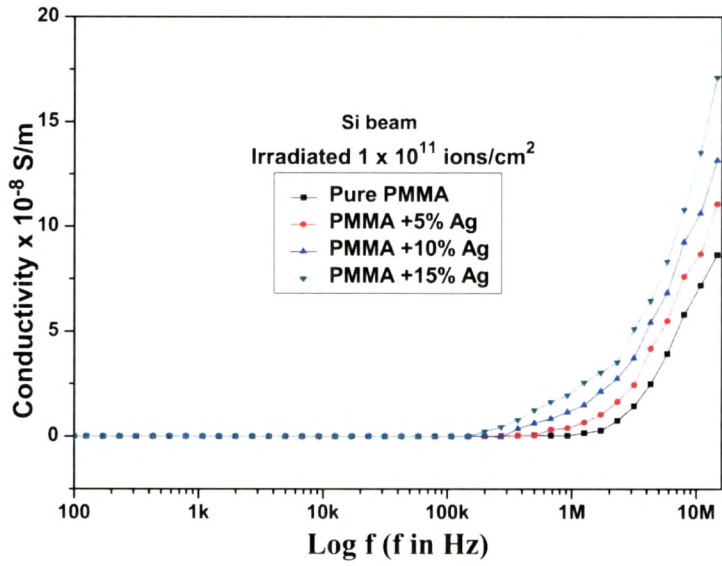
It was revealed that the conductivity increases with increasing concentration of dispersed nanoparticles and also with irradiation fluences. The increase in conductivity with different concentrations of silver nanoparticles for pristine samples may be attributed to the conductive phase formed by dispersed nanoparticles in polymer matrix. It is known that electrical conductivity of such composites depends on the type and concentration of the dispersed compound [19, 20]. It is also observed that the conductivity increases upon irradiation. Irradiation is expected to promote the metal to polymer bonding and convert the polymeric structure in to a hydrogen depleted carbon network. It is this carbon network that is believed to make the polymers more conductive [18].



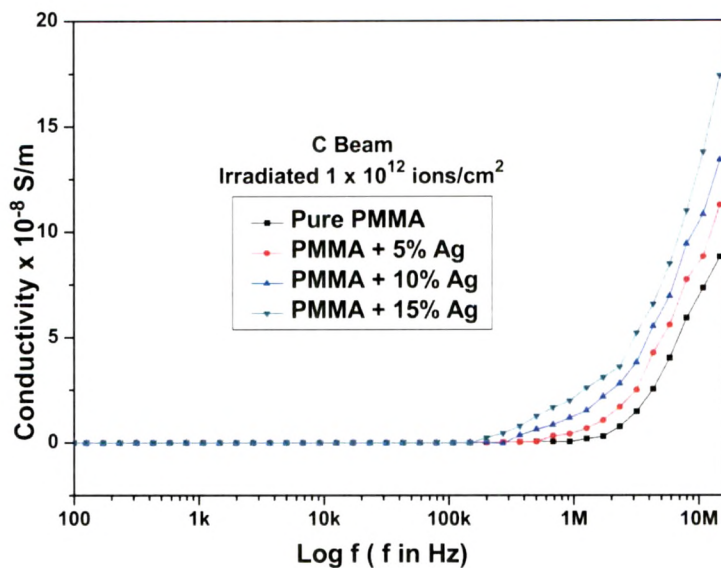
(a)



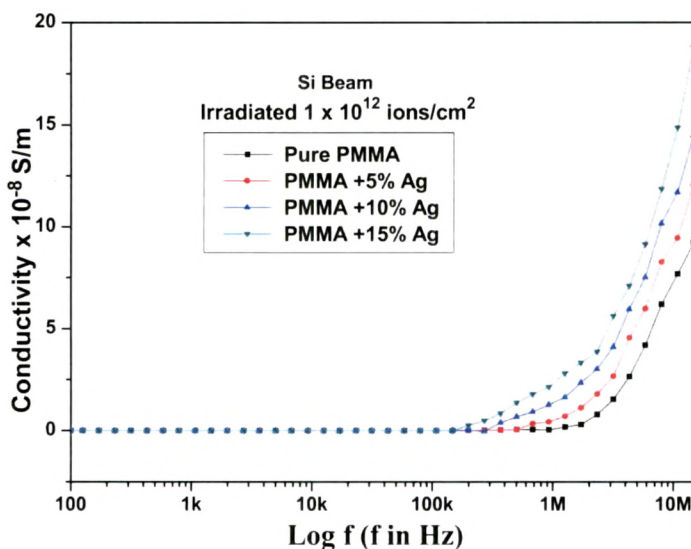
(b)



(c)



(d)



(e)

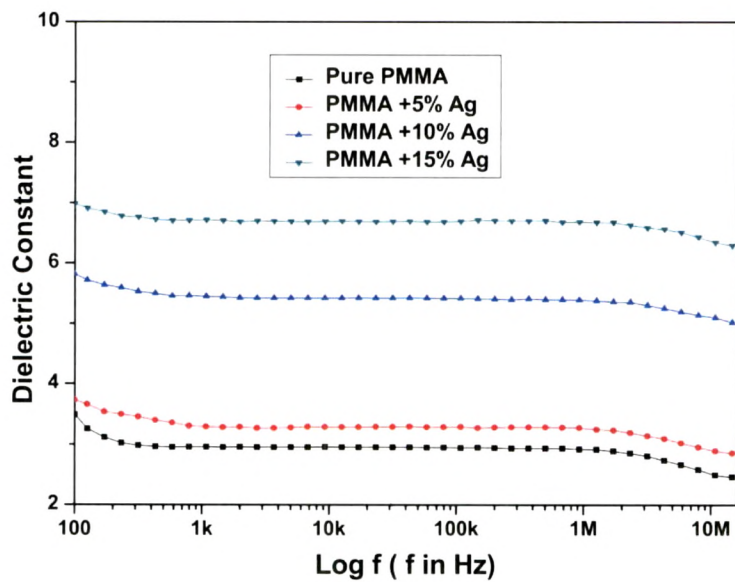
Fig. 3.5 Conductivity Vs Log f for (a) pristine (b) C beam (1×10^{11} ions/cm²) (c) C beam (1×10^{12} ions/cm²) (d) Si beam (1×10^{11} ions/cm²) (e) Si beam (1×10^{12} ions/cm²)

Dielectric properties of composites:

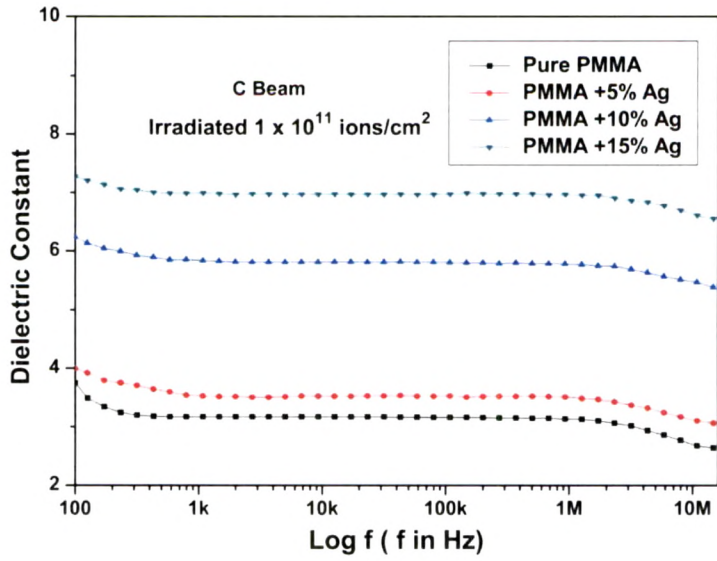
The variation of dielectric constant with respect to frequency for the PMMA/ silver nano particles composites at different filler concentrations are shown in Figure 3.6 (a-e). The effective dielectric constant in nanocomposites is determined by dielectric

polarization i.e. interfacial polarization between polymer and particles [21]. It is well recognized that nanocomposites have a huge volume fraction of interfaces where interfacial polarizations are most likely to occur. When the fillers are dispersed in the insulating polymer, the dielectric constant of composites increases with concentration of fillers [22].

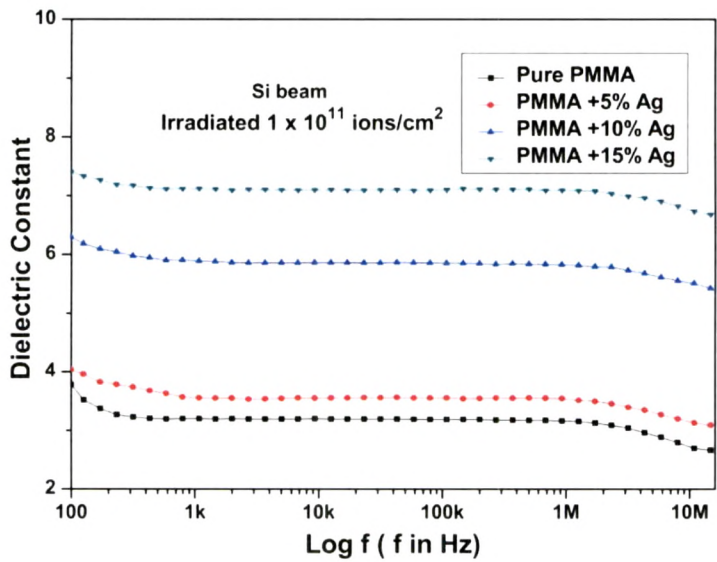
As apparent from Fig. 3.6, the dielectric constant remains almost constant up to 100 kHz. At these frequencies, the motion of free charge carriers may be assumed constant through the polymer matrix. Ion migration in solids is assumed to be dependent on the hopping rate *i.e.* the jumping frequency of the ions, which has a unique value for an ion. Therefore, the nearly constant value of dielectric constant may be due to the presence of some ionic species in excess amount [23]. It is also



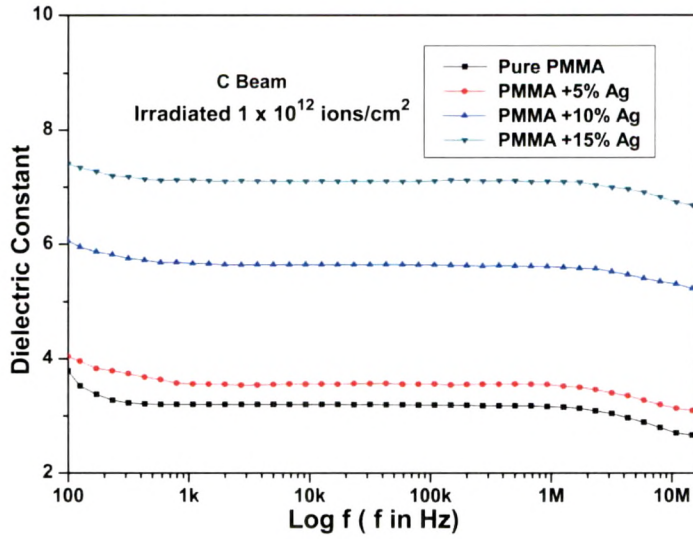
(a)



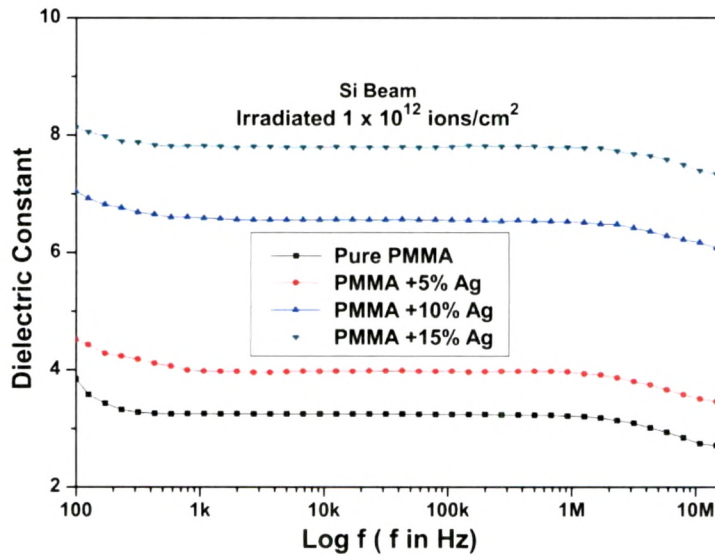
(b)



(c)



(d)



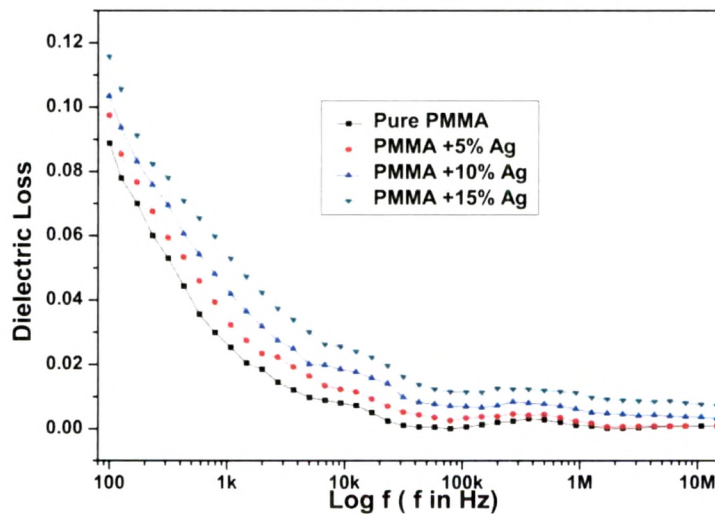
(e)

Fig. 3.6 Dielectric constant Vs Log f for (a) pristine (b) C beam (1×10^{11} ions/cm²) (c) C beam (1×10^{12} ions/cm²) (d) Si beam (1×10^{11} ions/cm²) (e) Si beam (1×10^{12} ions/cm²)

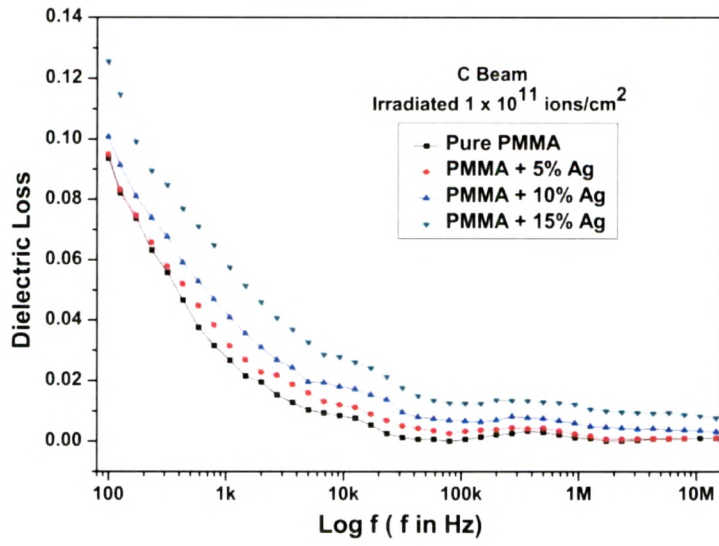
observed that dielectric constant increases for irradiated films. The increase in dielectric constant may be attributed to the chain scission and as a result the increase in the number of free radicals, unsaturation etc. As frequency increases further (i.e., beyond 100 kHz), the charge carriers migrate through the dielectric and get trapped

against a defect sites and induced an opposite charge in its vicinity. At these frequencies, the polarization of trapped and bound charges cannot take place and hence the dielectric constant decreases [24]. The observed nature of the fluence dependence of dielectric constant in studied frequency range can be explained by the prevailing influence of the enhanced free carriers due to irradiation [25].

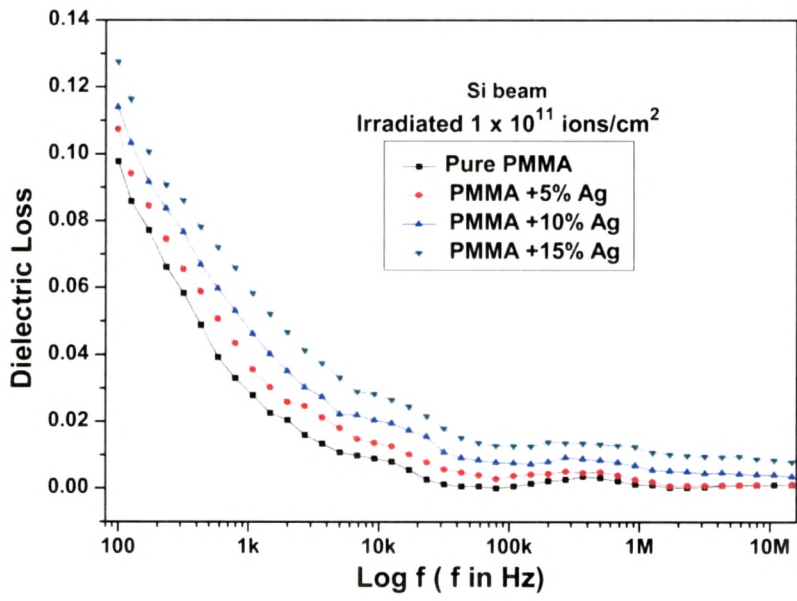
Fig. 3.7 (a-e) shows the variation of dielectric loss with log frequency for pristine and irradiated samples of pure PMMA and silver nanoparticles dispersed PMMA films at different concentrations. In general, the dielectric loss of the dielectric material causes from distortional, dipolar, interfacial, and conduction loss. The distortional loss is related to electronic and ionic polarization mechanisms. The interfacial loss created from the excessive polarized interface induced by the fillers and specifically the movement or rotation of the atoms or molecules in an alternating electric field. The conduction loss is featured to the dc electrical conductivity of the materials, representing the flow of actual charge through the dielectric materials [26].



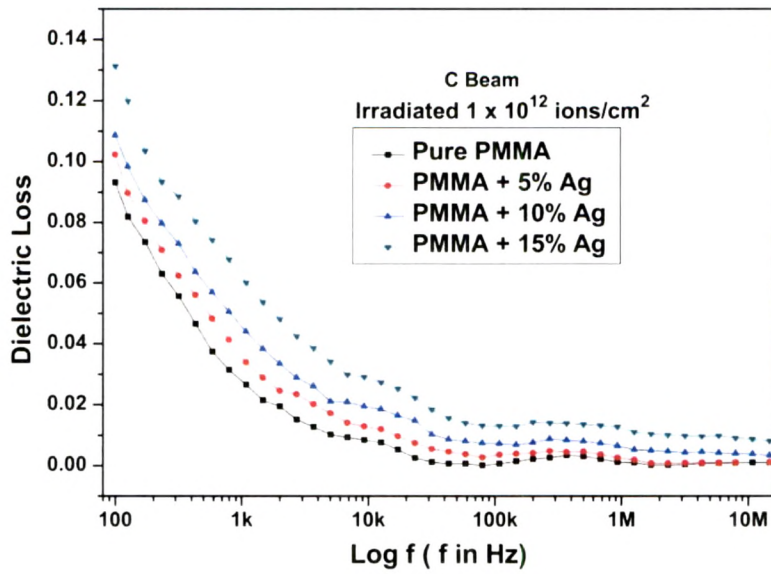
(a)



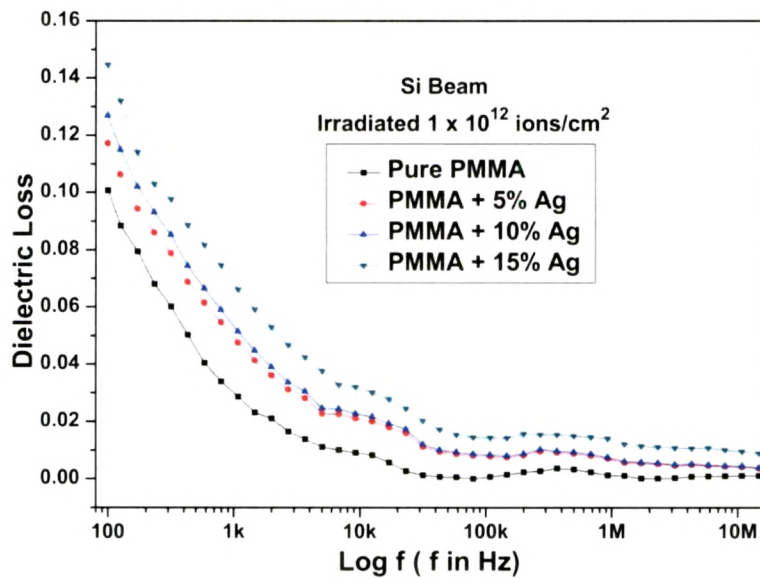
(b)



(c)



(d)



(e)

Fig. 3.7 Dielectric loss Vs Log f for (a) pristine (b) C beam (1×10^{11} ions/cm²) (c) C beam (1×10^{12} ions/cm²) (d) Si beam (1×10^{11} ions/cm²) (e) Si beam (1×10^{12} ions/cm²)

The dielectric loss decreases exponentially with the increase of log frequency. It is noticed that dielectric loss increases moderately with the concentration of filler and

also with upon both ion beams irradiations which may be attributed to the interfacial polarization mechanism of the heterogeneous system [26].

Conclusion:

Dispersion of silver nanoparticles in PMMA films has enhanced the properties of the pure polymer significantly. The increase in dielectric properties with different concentrations may be pointed to the conductive phase formed by dispersed nanoparticles in polymer matrix. Ion beam irradiation also has been shown to significantly enhance the dielectric properties which may be due to conversion of the polymeric structure into a hydrogen-depleted carbon network. It was found that the band gap value moved to lower energy (from 4.58 eV upto 3.21 eV) on doping with silver nanoparticles as well as upon irradiation from the UV- visible spectroscopy analysis. An XRD analysis reveals that the crystallite size of the samples decreased after ion beam irradiation which is also corroborated with the DSC analysis due to the chain scissioning upon irradiation. So we have concluded that effect of Si-beam is more effective than that of the C-beam because of large energy loss of heavy ion.

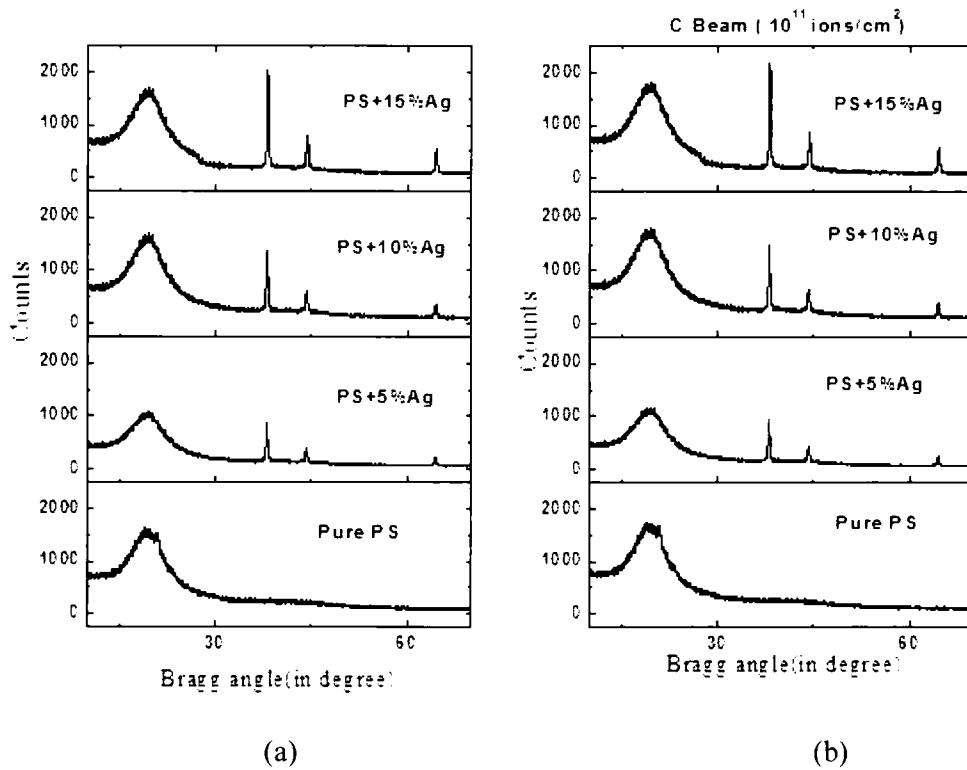
3.2 Effect of swift heavy ions irradiation on PS + Ag nanocomposites:

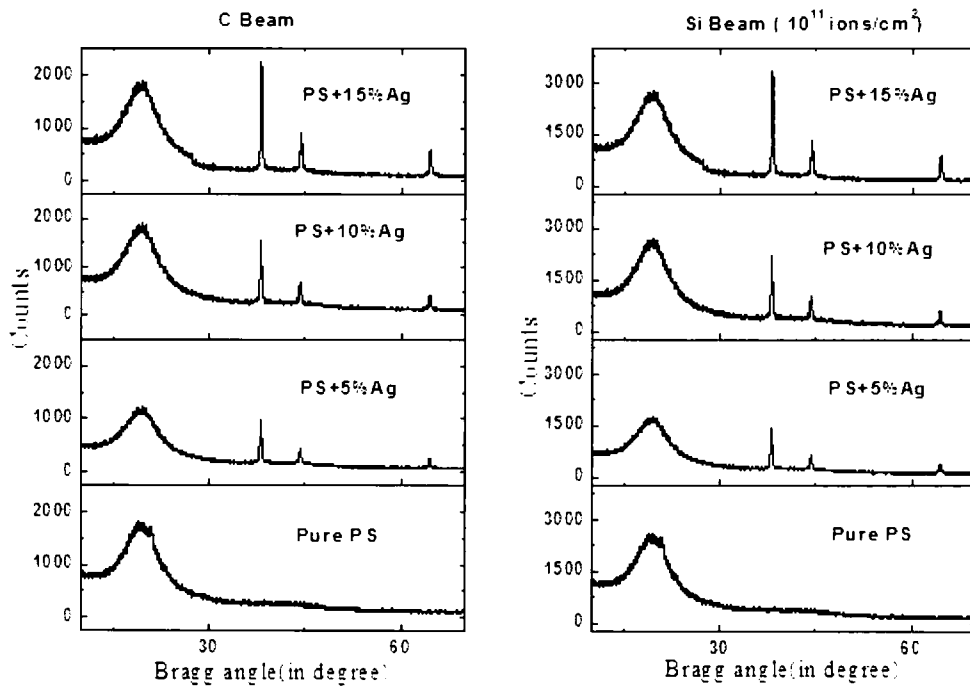
3.2.1 X-ray diffraction analysis:

The XRD patterns of composites are shown in Fig. 3.8(a-e). The figure clearly indicates that silver is crystalline, but the polymer is amorphous in nature and its composites show a semi-crystalline behavior. The diffraction patterns of the irradiated samples exhibited an increase in the peak intensity and a decrease in the full width at half-maximum (FWHM) corresponding to all observed peaks of silver. The average crystallite size (t) for pristine and irradiated samples was calculated using Scherrer's formula [9] as discussed in chapter 2 in section 2.3.1 from relation 2.2.3.

$$b = K\lambda / L \cos\theta$$

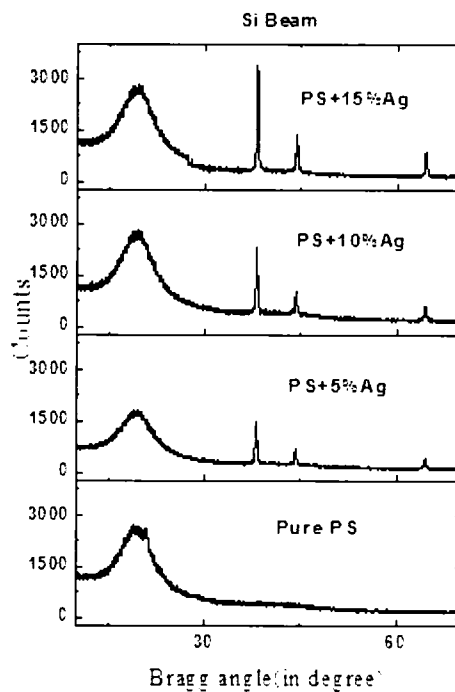
where b is FWHM in radians, λ is the wavelength of X-ray beam (1.5418 Å), L is the crystallite size in Å, K is a constant which varies from 0.89 to 1.39, but for most of the cases it is close to 1.





(c)

(d)



(e)

Fig. 3.8 X-ray diffraction patterns of (a) PS+ Ag (pristine) (b) C beam (1 x 10¹¹ ions/cm²) (c) C beam (1 x 10¹² ions/cm²) (d) Si beam (1 x 10¹¹ ions/cm²) (e) Si beam (1 x 10¹² ions/cm²)

Table 3.4 Crystallite size of pristine and irradiated samples

Sample	Pristine		C Beam		Si Beam	
	2 θ	Crystallite size (nm)	Crystallite size (nm) (1x10 ¹¹) ions/cm ²	Crystallite size (nm) (1x10 ¹²) ions/cm ²	Crystallite size (nm) (1x10 ¹¹) ions/cm ²	Crystallite size (nm) (1x10 ¹²) ions/cm ²
PS + 5%Ag	38.04	38.79	38.86	38.98	39.11	39.67
	44.22	36.95	37.18	37.95	37.89	38.19
	64.38	35.12	36.11	38.75	37.43	39.54
	Average	36.95	37.38	38.56	38.14	39.13
PS + 10%Ag	38.05	36.19	37.11	37.94	38.43	38.97
	44.21	38.13	38.21	38.54	38.45	39.58
	64.14	40.14	40.67	40.92	41.76	42.31
	Average	38.15	38.66	39.13	39.27	40.28
PS + 15%Ag	37.87	37.98	38.25	38.51	38.46	38.88
	44.11	37.87	38.01	38.19	38.34	38.90
	64.01	41.92	42.28	43.12	43.11	44.67
	Average	39.26	39.51	39.94	39.97	40.82

The crystallite size was calculated corresponding to the peak of the pristine and irradiated samples, and the results are listed in Table 3.4 [27]. It is observed that crystallite size increasing with filler concentrations and with irradiation fluence. The increase in crystallite size may be attributed to the cross linking phenomenon.

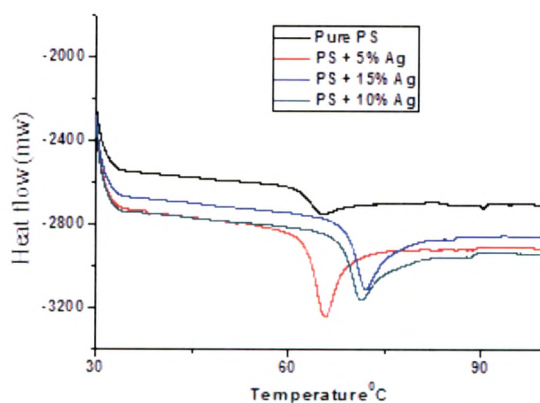
3.2.2. Thermal response (Differential scanning calorimetry (DSC)):

Fig.3.9 shows the influence of different concentrations of silver nanoparticles on the glass transition behavior of the polymer matrix. At the glass transition temperature, the weak secondary bonds that stick the polymer chains together are broken, and the macromolecule starts to move. The interaction of polymer chains and nanoparticle

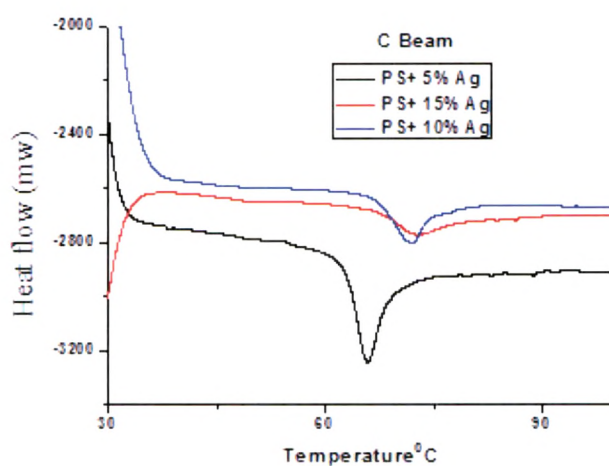
Table 3.5 Values of glass transition for pristine and irradiated composites

Sample name	Tg (Pristine)	Tg (C beam)	Tg (Si beam)
PS + 5 %Ag	65.2	65.7	66.2
PS + 10 %Ag	70.8	71.4	72.1
PS + 15 %Ag	71.9	72.7	73.2

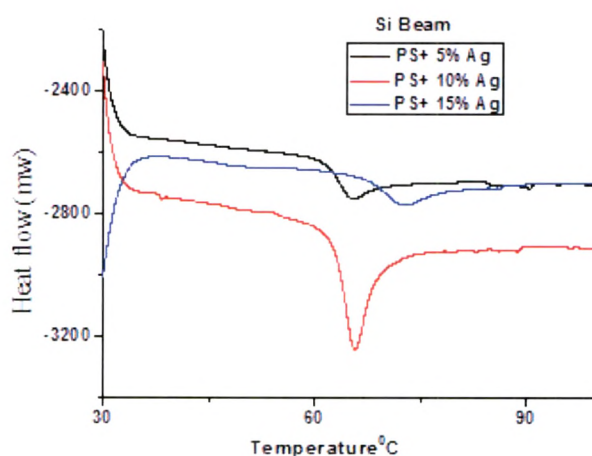
surfaces can alter the chain kinetics by decreasing or increasing the glass transition temperature of the polymer. T_g of pure PS is observed at 66.5°C. The T_g of pristine composite samples increased with filler contents and it further increased upon both ion beams irradiations to the higher temperature side as shown in Fig. 3.9 (a, b, c). This behavior probably arises due to branching (cross-linking effect) when islands of nanoparticles are bonded with polymeric chains. This lowers the mobility of the chains, and as a result, the glass transition temperature increases in the nanocomposites [28].



(a)



(b)



(c)

Fig. 3.9 DSC thermo grams for (a) pristine (b) Irradiated by C beam (1×10^{12} ions/cm²) (C) Irradiated by Si beam (1×10^{12} ions/cm²)

3.2.3 Optical response:

UV–vis spectroscopy is an important tool to investigate the value of optical band gap energy (E_g). The electronic transitions (\rightarrow) that are involved in the ultraviolet and visible regions are of the following type $\sigma \rightarrow \sigma^*$, $n \rightarrow \pi^*$, and $\pi \rightarrow \pi^*$ [29]. The

absorbance edge of the UV-vis spectra of pristine nanocomposites and irradiated by C ions and Si ions as shown in Fig.3.10. The absorbance in aromatic compounds is due to the π to π^* transition. This is very sensitive to the change in the environment around the phenyl ring [30]. It is observed that optical absorption increases with increasing energy loss and this absorption shifts from UV-vis towards the visible region for all irradiated nanocomposite samples. With increase of electronic energy loss the nanocomposites become gradually opaque to the visible light and the absorption edge shifts from UV to visible region. This is consistent with the observation that the material changes from transparent to opaque with increase of energy deposition. The increase in absorption with irradiation may be attributed to the formation of a conjugated system of bonds due to bond cleavage and reconstruction [31]. The shifting of absorption edge towards visible is generally considered to result from carbonization of the material under irradiation [32] which is also corroborated with the dielectric results.

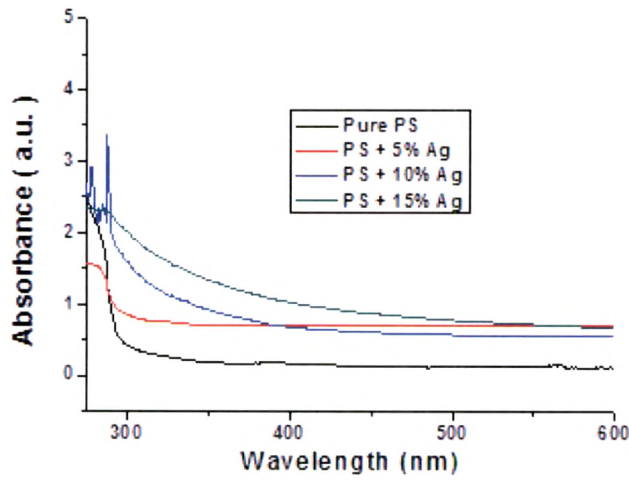
Determination of optical band gap:

Optical feature of the pristine and irradiated samples have been studied by Perkin-Elmer 25 Lambda UV-Visible spectroscope in the frequency range 200-800 cm^{-1} as illustrated in Fig. 3.10(a-e). The optical band gap E_g is obtained by tauc's equation [16] as discussed in chapter 2 in the section 2.3.3 by the relation 2.2.4.

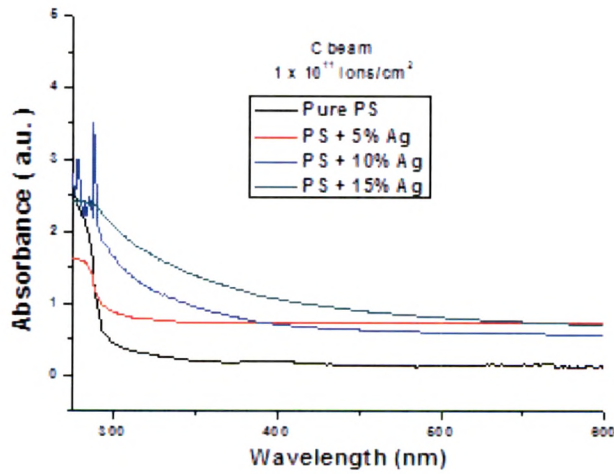
$$\text{i. e. } \omega\epsilon(\lambda) = (\hbar\omega - E_g)^2$$

Where $\epsilon(\lambda)$ is the optical absorbance and λ is the wavelength. The intersection of the extrapolated spectrum with the abscissa of the plot $\epsilon^{1/2}/\lambda$ versus $1/\lambda$, yields the gap wavelength λ_g from which the energy gap is derived as $E_g = hc/\lambda_g$. It is noticed that the band gap (energy gap) value shifted to lower energy from 4.38 eV upto 3.30 eV

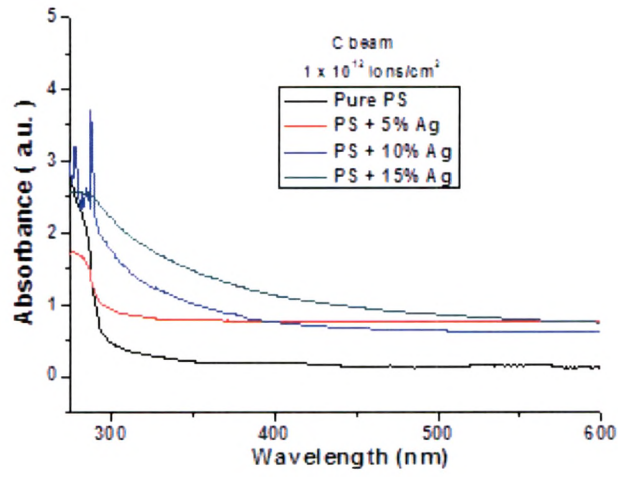
due to doping of silver nanoparticles and also upon irradiation by both ions beams. The decrease of the optical gap of ion-irradiated samples can be explained by the model of Robertson and O Reilly [33, 34]. They explained that the decrease in the band gap might be attributed to the transformation from separated aromatic rings to a structure similar to graphite with increasing fluences.



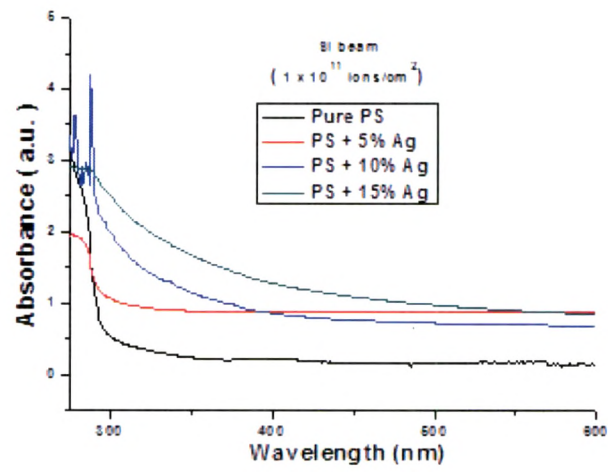
(a)



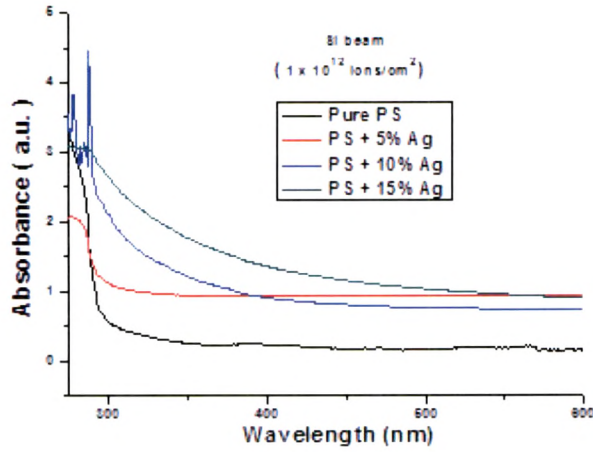
(b)



(c)



(d)



(e)

Fig. 3.10 Absorbance spectra of (a) Pristine (b) Irradiated by C beam (1×10^{11} ions/cm²) (c) Irradiated by C beam (1×10^{12} ions/cm²) (d) Irradiated by Si beam (1×10^{11} ions/cm²) (e) Irradiated by Si beam (1×10^{12} ions/cm²)

The number of carbon hexagon rings [33] in the cluster (M) is then found from the relation 2.2.6 as explained in chapter 2 in section 2.3.3.

$$E_g \approx 2 |\beta| / \sqrt{M}$$

Where, $|\beta|$ is a bond integral that represents the interaction energy of two π atomic orbitals. A theoretical value for $|\beta|$ proposed by Robertson and O Reilly is 2.9 eV, which according to Compagnini et al. [34] is an overestimation of the true value. So, the best-fit value of $|\beta|$ given by them is 2.2 eV. In the present study on the aromatic polymer, given equation has been used to calculate the value of M and its behaviour with different ions is summarized in Table 3.6. The number of rings (M) remains constant with the filler and upon irradiation except for Si-ions at a fluence of 1×10^{12} ions/cm².

Table 3.6 Band gap by direct allowed transitions, number of carbon atoms in pure PS, composites and irradiated films.

Sample	Pristine		C Beam		Si Beam	
	Band gap in eV	No. of carbon hexagon rings	Band gap in eV	No. of carbon hexagon rings	Band gap in eV	No. of carbon hexagon rings
Pure PS	4.38	~1	4.21	~1	3.89	~1
PS + 5%Ag (1 x 10 ¹¹ ions/cm ²)	4.33	~1	4.11	~1	3.89	~1
PS + 5%Ag (1 x 10 ¹² ions/cm ²)	4.28	~1	3.90	~1	3.87	~1
PS + 10%Ag (1 x 10 ¹¹ ions/cm ²)	4.21	~1	3.88	~1	3.70	~1
PS + 10%Ag(1 x 10 ¹² ions/cm ²)	4.15	~1	3.78	~1	3.50	~1
PS + 15%Ag (1 x 10 ¹¹ ions/cm ²)	4.10	~1	3.70	~1	3.44	~1
PS + 15%Ag(1 x 10 ¹² ions/cm ²)	3.90	~1	3.60	~1	3.30	~2

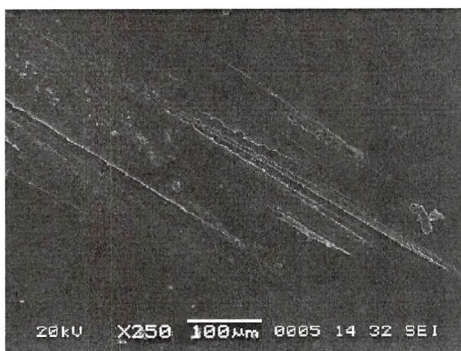
3.2.4 Surface morphology:

Fig. 3.11(a-e) shows the SEM images of pristine, composites and irradiated composite films with magnification of X250. The analysis shows that the filled particles are distributed randomly in the matrix which display continuous contact between themselves and formed conducting paths. The surface becomes smoothen upon irradiation. The decrease in roughness with Ag-nanoparticles may be attributed

to the decrease in density of metal particles on the surfaces of the films, which is also responsible for increase in crystallinity of the material as indicated by XRD analysis.



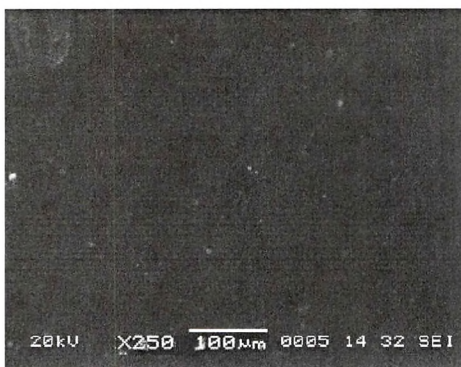
(a)



(b)



(c)



(d)

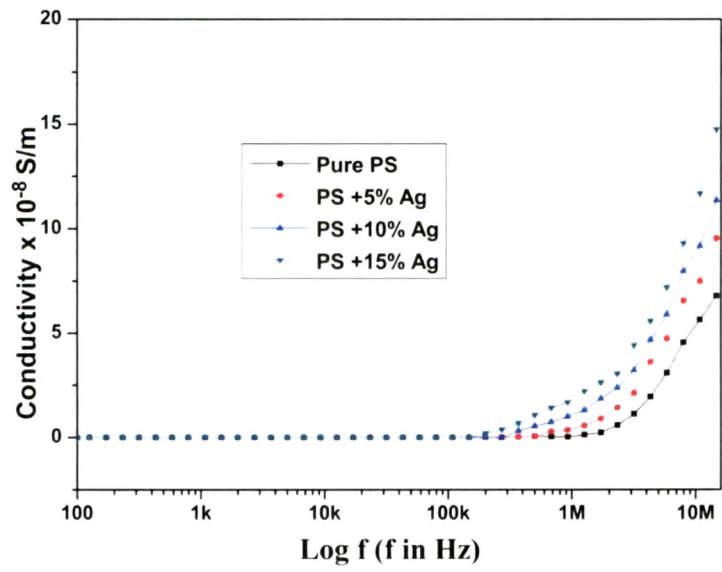


(e)

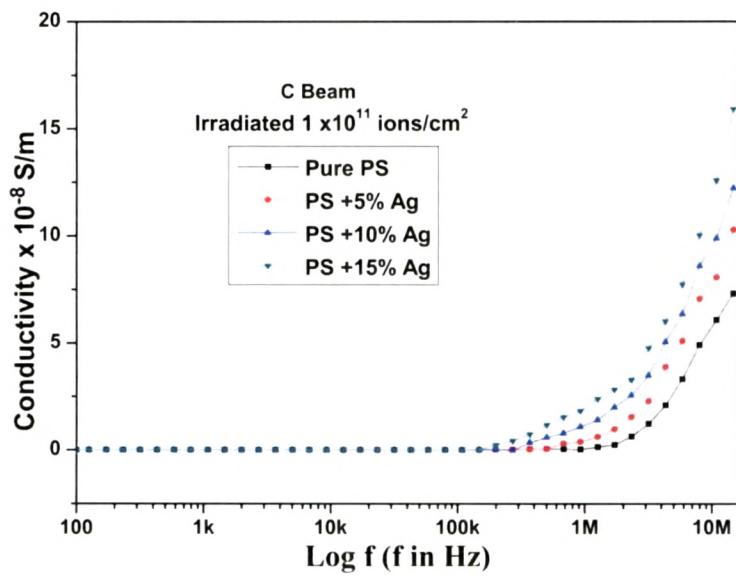
Fig. 3.11 SEM Images for (a) Pure PS (b) PS irradiated (C beam) (c) PS+15% Ag (d) PS+15% Ag (C Beam) (e) PS+15% Ag (Si beam)

3.2.5 AC electrical frequency response:

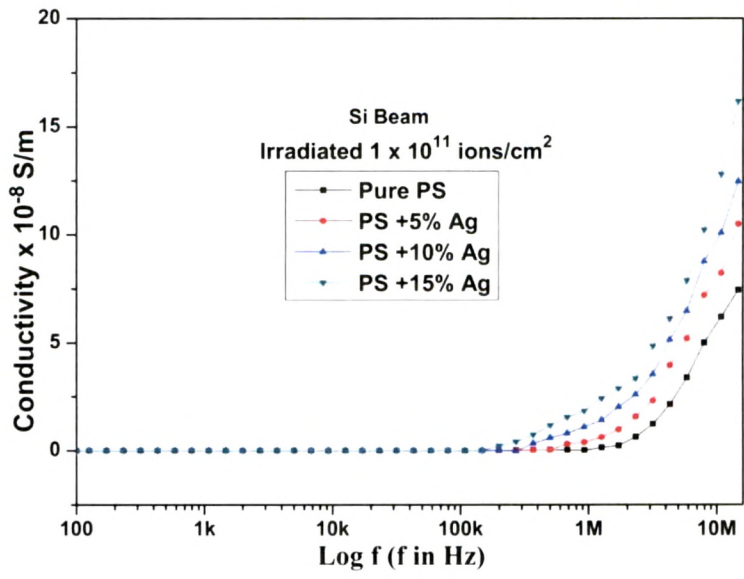
Conductivity: Fig. 3.12(a-e) shows the frequency dependent ac electrical conductivity of pristine and irradiated composites. The increase in conductivity with silver nanoparticles concentration for pristine samples may be attributed to the conductive phase formed by dispersed metal nanoparticles in polymer matrix. It is known that electrical conductivity of such composites depends on the type and concentration of the dispersed compound [20, 21]. The increase in conductivity is related to a possible increase in the number of conduction paths created between the filler particles aggregates in the composite and as a consequence electrical path in the polymer matrix in addition to a decrease in the width of the potential barriers within the bulk region of high conductivity. Therefore more charge carriers may be able to ‘hop’ by tunneling, resulting in the increase in the bulk conductivity and it also increases with increasing filler concentration [19]. Conductivity is further observed to increase upon irradiation. Irradiation is expected to promote the metal to polymer bonding and convert polymeric structure into hydrogen depleted carbon network. It is this carbon network that is believed to make the polymer more conductive [27].



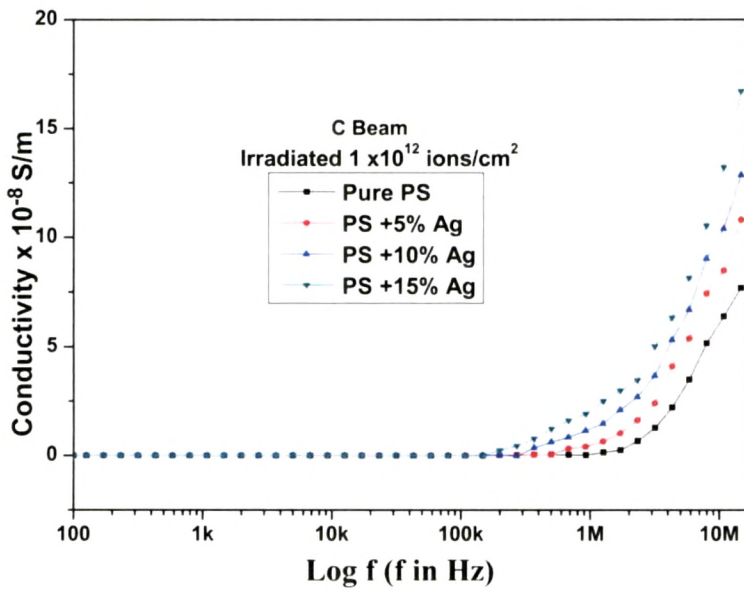
(a)



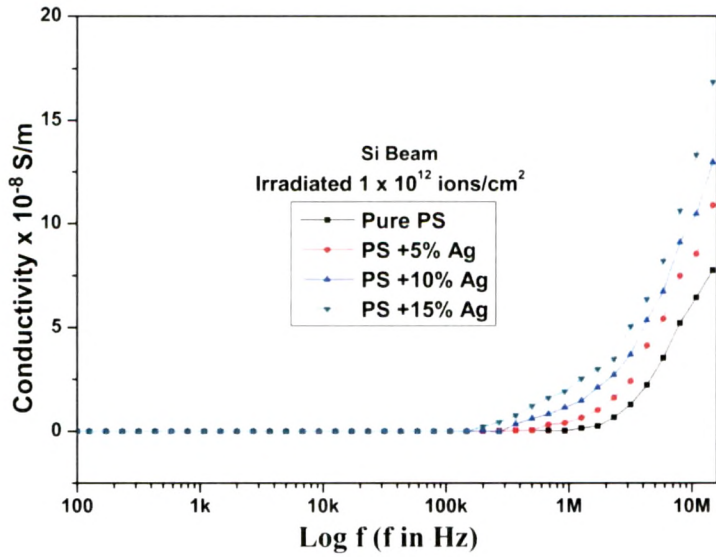
(b)



(c)



(d)

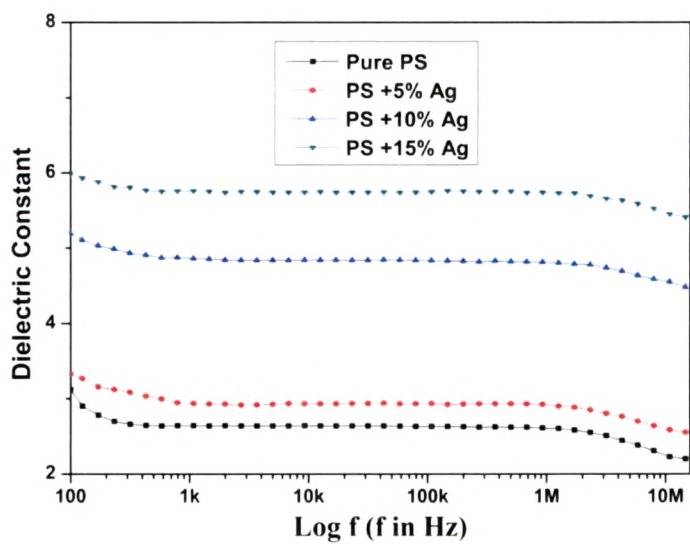


(e)

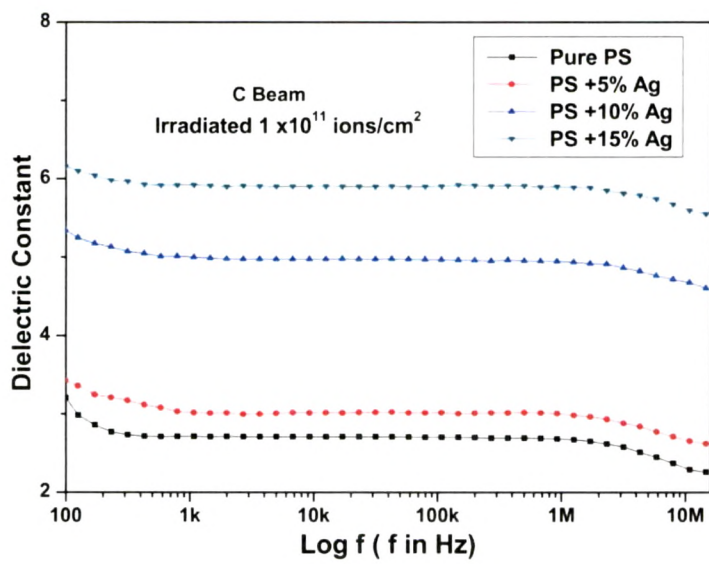
Fig. 3.12 Conductivity Vs Log f for (a) pristine (b) C beam (1×10^{11} ions/cm²) (c) Si beam (1×10^{11} ions/cm²) (d) C beam (1×10^{12} ions/cm²) (e) Si beam (1×10^{12} ions/cm²)

Dielectric property of composites:

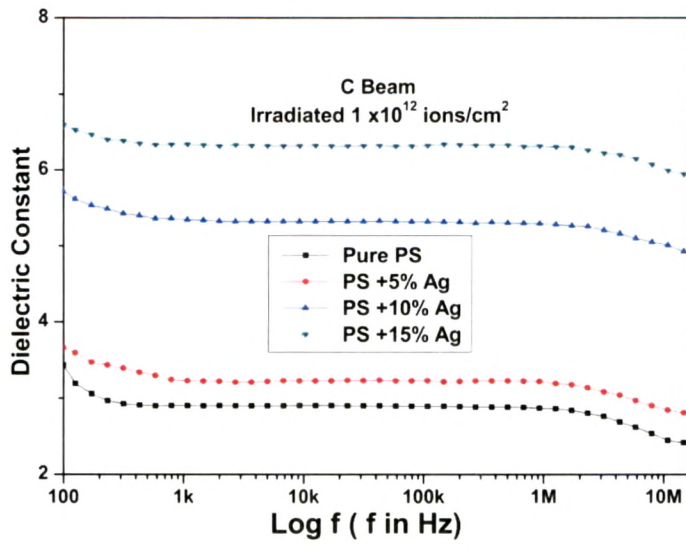
Fig. 3.13 (a-e) shows the dependence of the dielectric constant on the frequency of the applied field at different filler concentrations and irradiation fluences. It is observed that the dielectric constant decreases at high frequency; this is thought to be caused by the slow dielectric relaxation of the matrix and the interface of the composite [33]. At these frequencies, the charge carriers roam through the dielectric and get trapped against a defect site, inducing an opposite charge in their vicinity, and as a result, the motion of charge carriers is slowed down and the value of the dielectric constant decreases. According to the Dissado and Hill theory, in intra-



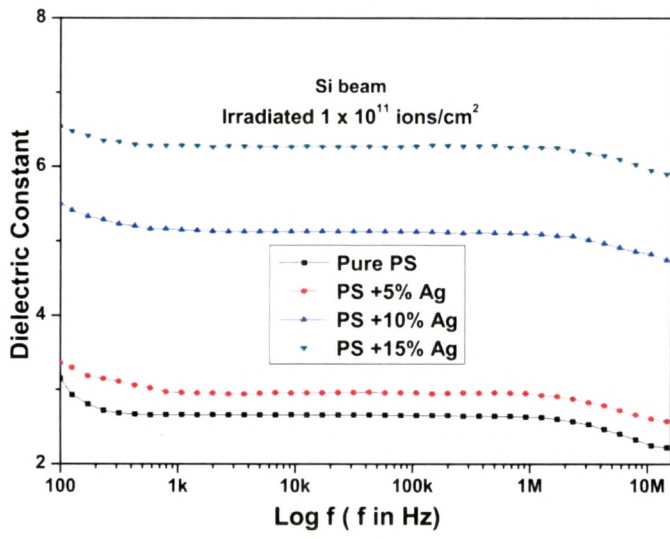
(a)



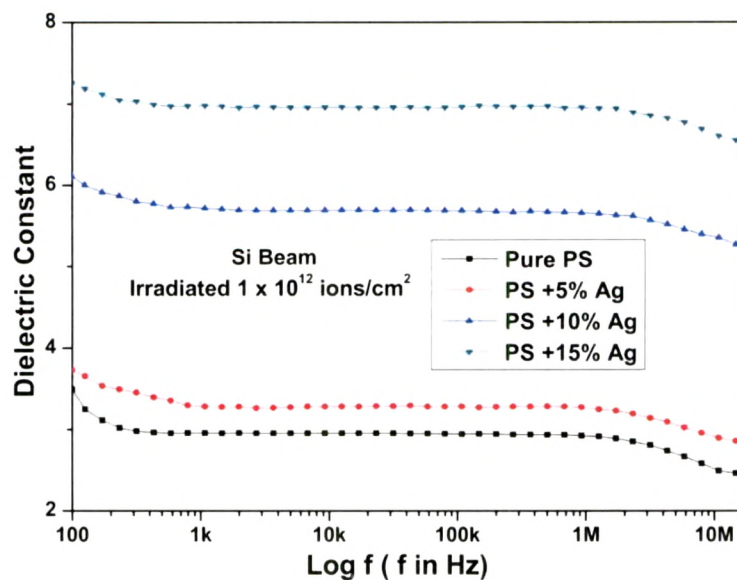
(b)



(c)



(d)



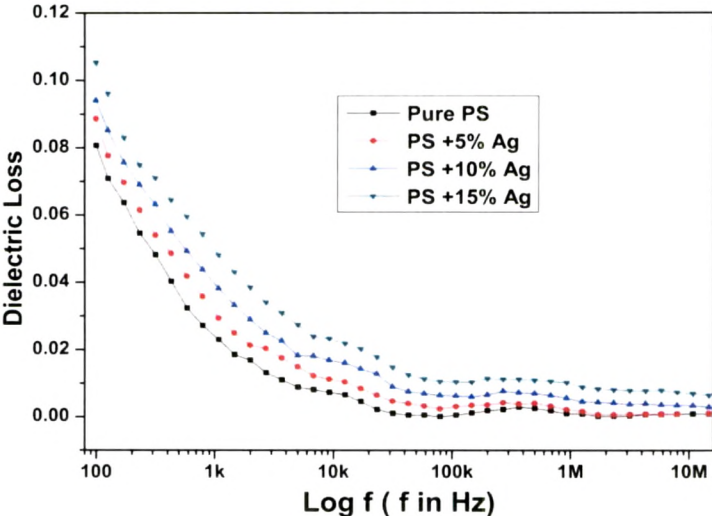
(e)

Fig. 3.13 Dielectric Constant Vs Log f for (a) pristine (b) C beam (1×10^{11} ions/cm²) (c) C beam (1×10^{12} ions/cm²) (d) Si beam (1×10^{11} ions/cm²) (e) Si beam (1×10^{12} ions/cm²)

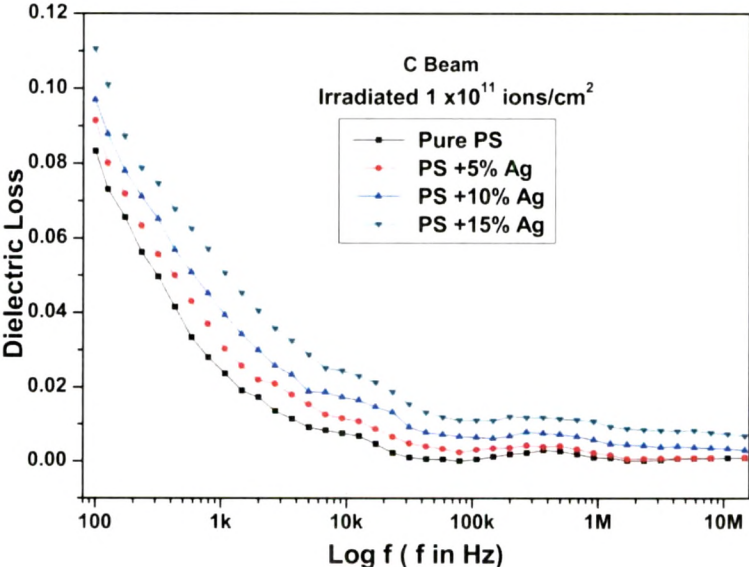
cluster motions, the relaxation of a dipole will produce a ‘chain’ response in its neighboring dipoles and the reaction of the neighboring dipoles will, in turn, affect the first dipole, so the overall effect will be seen as a single-cluster dipole moment relaxation. This reduces the dielectric constant at these frequencies [35]. There is an increase in the dielectric permittivity with metal concentrations as the quantity of accumulated charges increases because of the polarization of polymer/metal at the interfaces. The polarization makes an additional contribution to the charge quantity. The increase in the dielectric constant upon irradiation may be attributed to the chain scission, which results in an increase in free radicals, unsaturation, etc., when compared with the pristine samples [36].

The dielectric loss decreases exponentially first, then becomes less dependent on the frequency. This is because the induced charges gradually fail to follow the reversing

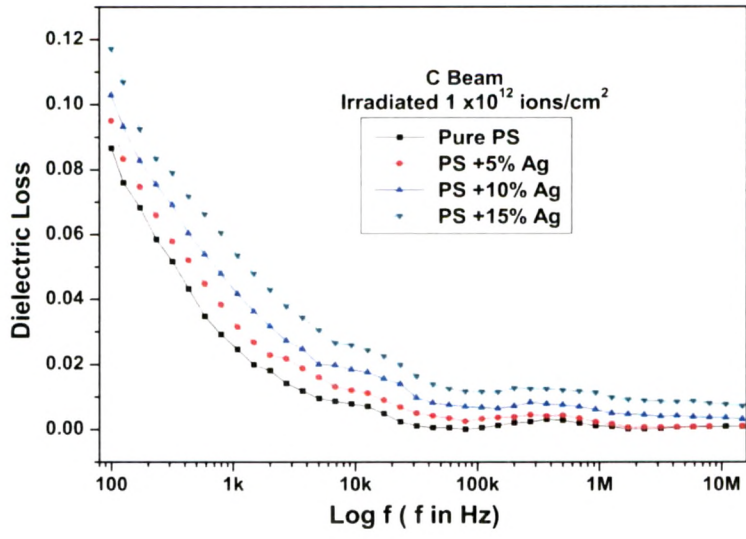
field, causing a reduction in the electronic oscillations as the frequency is increased. The dielectric loss also increases moderately with filler contents and with irradiation fluence also, as shown in Fig. 3.14 (a-e) [37]. The increase in the dielectric loss may be attributed to the interfacial polarization mechanism of the heterogeneous system.



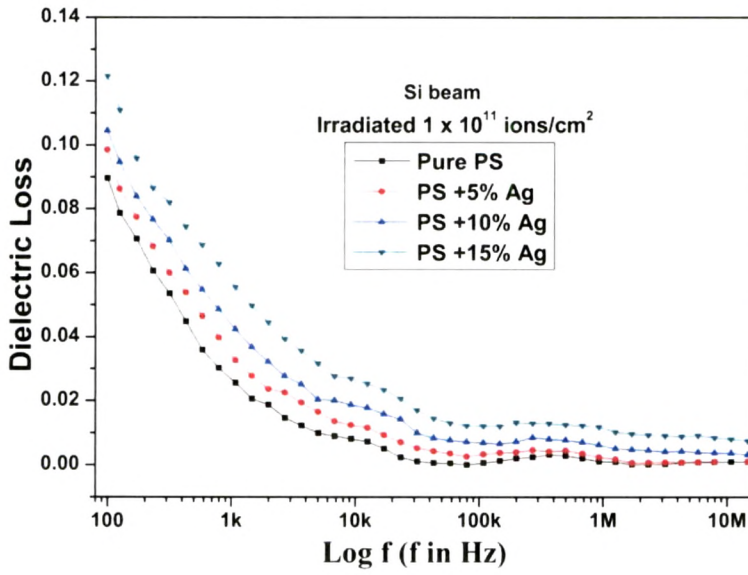
(a)



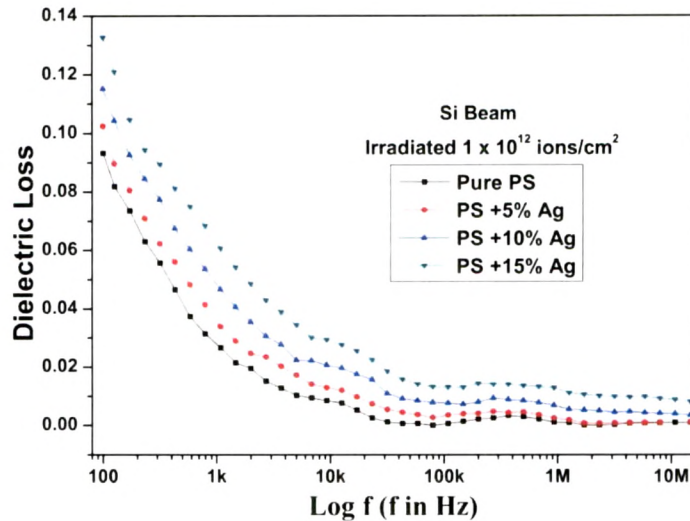
(b)



(c)



(d)



(e)

Figure 3.14 Dielectric loss Vs Log f for (a) pristine (b) C beam (1×10^{11} ions/cm²) (c) C beam (1×10^{12} ions/cm²) (d) Si beam (1×10^{11} ions/cm²) (e) Si beam (1×10^{12} ions/cm²)

Conclusion:

Dispersion of silver nanoparticles in PS films has enhanced the properties of the pure polymer significantly. The increase in dielectric properties with different concentrations may be pointed to the conductive phase formed by dispersed nanoparticles in polymer matrix. Ion beam irradiation also has been shown to significantly enhance the dielectric properties may be due to conversion of the polymeric structure into a hydrogen-depleted carbon network. It was found that the band gap value moved to lower energy (from 4.38 eV upto 3.30 eV) on doping with silver nanoparticles as well as upon irradiation as revealed from the UV- visible spectroscopy analysis. An XRD analysis reveals that the crystallite size of the samples increased after ion beam irradiation which is also corroborated with the DSC analysis due to the crosslinking upon irradiation.

3.3 Summary

Two different composites have been studied using two different ion beams (C and Si) irradiations. Structural, optical, electrical properties and surface morphology have been examined by different characterization techniques.

XRD analysis; the results show that the crystallite size of fillers decreases slightly upon both ion beams irradiations in PMMA nanocomposites. It is also observed that the intensity of the peak decreases and to some extent broadening of the peak after irradiation offers confirmation of decrease in crystallinity. Since no significant change in the peak position is observed, this reveals that lattice parameters do not change significantly in both irradiations. Rather in the case of PS nanocomposites, crystallite size of fillers increases upon both ion beams irradiations which may be attributed to cross linking effect.

DSC thermograms analysis reveals that the T_g value decreases upon irradiations in PMMA nanocomposites and increases upon irradiations in PS nanocomposites. This behavior probably arises due to branching (cross-linking effect) when islands of nanoparticles are bonded with polymeric chains. This lowers the mobility of the chains, and as a result, the glass transition temperature increases in the nanocomposites. Decrease in T_g was explained by thin film model. When the inter-particles distance is small enough, then the polymer between two particles can be considered as a thin film. Assuming that there is small or no interfacial interaction between the filler and matrix exists and then T_g decreases.

UV-Vis analysis; the band gap values for both composites were increased upon concentration of fillers and both ions irradiations. It was observed from the UV-visible spectroscopy analysis that the band gap value moved to the lower energy.

Surface morphology; SEM images showed that increase in density in PMMA nanocomposites and decrease in density in PS nanocomposites upon irradiations.

Dielectric properties; Ac electrical conductivity of all pristine and irradiated samples at different filler concentrations is shown in Fig.3.15. The increase in conductivity with silver nanoparticles concentration for pristine samples may be attributed to the conductive phase formed by dispersed metal nanoparticles in polymer matrix. The increase in conductivity is related to a possible increase in the number of conduction paths created between the filler particles aggregates in the composite and as a consequence electrical path in the polymer matrix in addition to a decrease in the width of the potential barriers within the bulk region of high conductivity. Therefore more charge carriers may be able to 'hop' by tunneling, resulting an increase in the bulk conductivity and it also increases with increasing filler concentration. Conductivity is further observed to increase upon irradiation. Irradiation is expected to promote the metal to polymer bonding and convert polymeric structure into hydrogen depleted carbon network. It is this carbon network that is believed to make the polymer more conductive. Fig 3.15 shows comparison of conductivity of all composites before and after irradiation. For the sake of comparison filler concentration (5, 10, 15 wt%) at a fluence of 1×10^{12} ions/cm² for C and Si ions beams at a frequency of 10 MHz have considered. In Fig 3.16, similar comparison has also been made for dielectric constant of all composites.

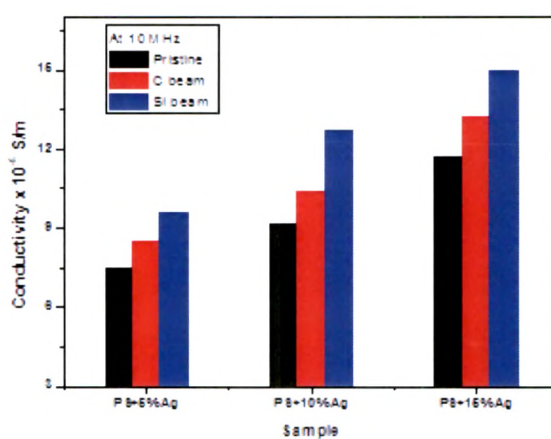
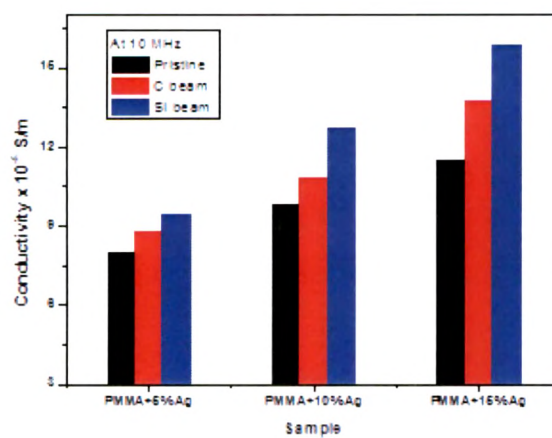


Fig. 3.15 Comparison of conductivity of pristine and irradiated samples at 10 MHz

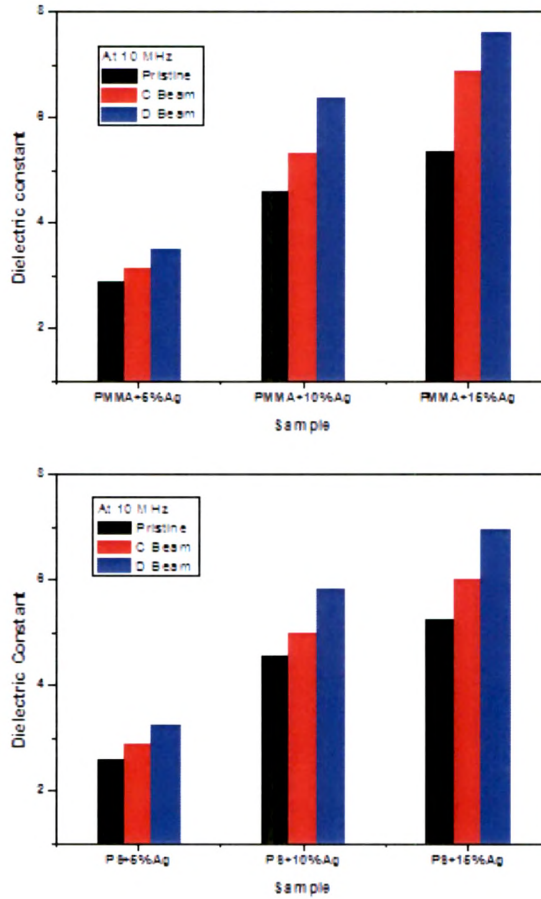


Fig. 3.16 Comparison of dielectric constant of pristine and irradiated samples at 10 MHz

Fig. 3.16 shows the dependence of the dielectric constant on the frequency of the applied field at different filler concentrations and irradiation fluences.

In all the cases, it reveals that dielectric loss is positive and signifies inductive behaviour of the material.

References:

- [1] Lin Bin, A. Gelves Genaro, A. Haber Joel, and Sundararaj Uttandaraman, *Ind. Eng. Chem. Res.*, 46 (2007) 2481-2487.
- [2] A. Gelves Genaro, Sundararaj Uttandaraman, A. Haber Joel, *Macromol. Rapid Commun.*, 26 (2005)1677–1681.
- [3] K. Singh Samra, S. Thakur, L. Singh, *Nuclear Instruments and Methods in Physics Research B* 269 (2011) 550–554.
- [4] Kawaljeet Singh Samra, Sonika Thakur, Lakhwant Singh, *Nuclear Instruments and Methods in Physics Research B*, 269 (2011) 550–554.
- [5] Chaitali Gavade, N. L. Singh, D. K. Avasthi, Alok Banerjee, *Nuclear Instruments and Methods in Physics Research B*,268(2010) 3127–3131.
- [6] R. Kumaravel, K. Ramamurthi, Indra Sulania, K. Asokan, D. Kanjilal, D. K. Avasti, P. K.Kulria, *Radiation Physics and Chemistry*, 80 (2011) 435–439.
- [7] Chaitali Gavade, N. L. Singh, P. K. Khanna, *Journal of Nanoscience and Nanotechnology*, 14 (2014)1.
- [8] Chaitali Gavade, N. L. Singh, Anita Sharma, P. K. Khanna, Fouran Singh, *Radiation Effects & Defects in Solids*,166 (2011) 585–591.
- [9] P. Scherrer, *Gott Nachar*, 2 (1918) 98–100.
- [10] R. Kumar, U. De, R. Prasad, *Nucl. Instrum. Methods B* 248 (2006) 279-283.
- [11] V.V. Vodnik , D.K. Bozanic, E. Dzumuzovic, J. Vukovic, J.M. Nedeljkovic, *European Polymer Journal* 46 (2010) 137.
- [12] B. J. Ash, L. S. Schadler, R. W. Siegel, *Mater Lett* 55 (1–2) (2002) 83.
- [13] D. L. Pavia, G.M. Lampman, G.S. Kriz, *Introduction to Spectroscopy*, Harcourt College Publishers, Philadelphia (2001).
- [14] A. K. Srivastava, H. S. Virk, *J. Polym. Mater.* 17 (2000) 325.

- [15] H S Virk , P S Chandi And A K Srivastava, Bull. Mater. Sci. 24(5) (2001) 529.
- [16] A. Das, S. Dhara and A. Patnaik Physical Rev B 59 (1999) 11069.
- [17] Anjum Qureshi , Dolly Singh , N.L. Singh, S. Ataoglu , Arif N. Gulluoglu , Ambuj Tripathi ,D.K. Avasthi, Nuclear Instruments and Methods in Physics Research B 267 (2009) 3456.
- [18] S. Shah, N.L. Singh, A. Qureshi, D. Singh, K.P. Singh, V. Shrinet, A. Tripathi, Nucl. Instrum. Methods B 226 (2008) 1768-1774.
- [19] M. Abu-Abdeen, G. M. Nasr, H. M. Osman, A. I. Abound, Egypt J. Sol. 25 (2002) 275-294.
- [20] Ye. P. Mamunya, V. V. Davydenko, P. Pissis, E. V. Lebedev, Eur. Polymer Journal 38 (2002) 1887-1897.
- [21] Santanu Singh, M. Joy Thomas, IEEE Transactions on Dielectrics and Electrical Insulation 15(1) (2008) 2-11.
- [22] Rajesh Kumar, S Asad Ali, Udayan De, D K Avasthi and Rajendra Prasad, Indian J. Phys. 83 (7) (2009) 963-968.
- [23] A.K. Jonscher, Dielectric Relaxation in Solids; Chesla Dielectric Press: London, 1983.
- [24] T. Phukan, D. Kanjilal, T. D. Goswami, Nucl. Instr. And Meth. B 234 (2005) 520-524.
- [25] Jiongxin Lu, Kyoung-Sik Moon, Jianwen Xu, C. P. Wong, J. Mater. Chem.16 (2006) 1543-1548.
- [26] N. L. Singh, Sejal Shah , Anjum Qureshi , K. P. Singh , V. Shrinet , P. K. Kulriya , A. Tripathi Radiation Effects & Defects in Solids 163(2) (2008) 169-177.
- [27] D. Singh, N.L. Singh, A. Qureshi, P. Kulriya, A. Tripathi, D.K. Avasthi, A.N. Gulluoglu, J. Non-Cryst. Solids, 356 (2010) 856–863.

- [28] X. Yan, T. Xu, S. Xu, S. Wang, *Nanotechnology*, 15 (2004) 1759–1762.
- [29] Rajesh Kumar, S. Asad Ali, A.K. Mahur, H.S. Virk, F. Singh, S.A. Khan, D.K. Avasthi, Rajendra Prasad, *Nuclear Instruments and Methods in Physics Research B* 266 (2008) 1788–1792.
- [30] S. Saravanana, M.R. Anantharaman, S. Venkatachalam, D.K. Avasthi, *Vacuum* 82 (2008) 56–60.
- [31] L.S. Farenza, R.M. Papaleo, A. Hallen, M.A. Araujo, R.P. Livi, B.U.R. Sundqvist, *Nucl. Instr. and Meth. B* 105 (1995) 134.
- [32] Zhiyong Zhu, Yunfan Jin, Changlong Liu, Youmei Sun, Mingdong Hou, Chonghong Zhang, Zhiguang Wang, Jie Liu, Xiaoxi Chen, Baoquan Li, Yanbin Wang, *Nuclear Instruments and Methods in Physics Research B* 169 (2000) 83–88.
- [33] A. Das, S. Dhara and A. Patnaik *Physical Rev B* 59 (1999) 11069.
- [34] J. Robertson, E.P. O Reilly, *Phys. Rev. B* 35 (1987) 2946.
- [35] G. Sui, S. Jana, W. H. Zhong, M. A. Fuqua, C. A. Ulven, *Acta Mater.*, 56 (2008) 2381–2388.
- [36] N. L. Singh, S. Shah, A. Qureshi, K. P. Singh, V. Shrinet, A. Tripathi, *Radiat. Eff. Def. Solids* (163)(2) (2008) 169–177.
- [37] A. Qureshi, N. L. Singh, S. Shah, F. Singh, D.K. Avasthi, *J. Macromol. Sci.* (45) (2008) 265–270.
- [38] S. Shah, D. Singh, A. Qureshi, N. L. Singh, K. P. Singh, V. Shrinet, *Indian J. Pure Appl. Phys.* (46) (2008) 439–442.